JOURNAL OF MAGNETIC RESONANCE **128,** 172–193 (1997)
ARTICLE NO. MN971219

Broadband Polarization Transfer under Magic-Angle Spinning: Application to Total Through-Space-Correlation NMR Spectroscopy

M. Baldus and B. H. Meier

NSR-Center for Molecular Structure, Design and Synthesis, Laboratory of Physical Chemistry, University of Nijmegen, Toernooiveld 6525 ED Nijmegen, The Netherlands

Received February 17, 1997; revised July 10, 1997

A pulse sequence is described that leads to a broadband recoupling of the dipolar interaction in magic-angle-spinning solid-state NMR experiments of ^{13}C spins. The sequence is based on a combination of rotating frame and laboratory frame transfer periods. The recovered dipolar interaction is only weakly dependent on spectral parameters but is a faithful measure for the internuclear distances. Furthermore, a pure zero-quantum term is recovered (of the type found in static ''spin-diffusion'' experiments). This makes the pulse sequence particularly suited for incorporation into two-dimensional total through-space correlation experiments that deliver simultaneous information about all dipolar couplings in a single 2D experiment. It is found that the necessary decoupling from abundant protons is best performed in two steps: first, the strong homonuclear couplings between the high-γ spins are averaged by Lee–Goldburg irradiation and, second, the heteronuclear dipolar interaction is averaged by the combined application of an RF field to the low-γ spins and magic-angle sample spinning. Phase-inversion and amplitude attenuation in the rotating frame and refocusing pulses in the laboratory frame part of the pulse sequence are introduced to achieve an optimum chemical-shift offset-independence and for the suppression of unwanted double-quantum transitions. The design principles are explained in detail. Finally, the pulse scheme is applied to total-correlation spectroscopy of a uniformly labeled amino acid. The experimental cross-peak intensities are in qualitative agreement with the known crystal structure of the model compound.

1. INTRODUCTION

Multidimensional NMR is an important tool for structure elucidation in a variety of applications in liquid (*1, 2*), liquid-crystalline, and solid phase (*3*). In the liquid state, structural information from small and medium-sized molecules (<30 kDa) is usually obtained using a combination of through-space (*4*) and through-bond (*5, 6*) experiments. These experiments require that the resonance lines of the involved spins are spectrally resolved and cross peaks between them can be observed. A similar approach can be attempted in the solid phase where the dipolar interaction is part of the secular spin Hamiltonian and the dipolar information can be obtained by a total through-space correlation experiment. The classification ''through-space'' and ''through-bond'' interactions is determined on grounds of the type of interactions; dipolar transfer between covalently bond nuclei is denoted as ''through space.'' In the liquid state, the dipolar interaction is averaged out by the molecular tumbling of the individual molecules but remains observable through cross-relaxation effects.

Sufficient spectral resolution is sometimes difficult to achieve in the solid phase, and usually, the application of magic-angle spinning (MAS) (*7*) is mandatory to remove the chemical-shielding anisotropy. MAS does, however, remove the dipolar interaction and therefore destroys the through-space-distance information. A number of ''recoupling'' schemes have been proposed to interfere with the MAS averaging process and to at least partially recover the dipolar interaction:

Frequency-selective through-space MAS polarization transfer between spins whose resonance offsets differ by a multiple of the MAS spinning frequency can be achieved without the application of pulses to the observed spins (*8–11*). Attempts have been made to broaden this rather narrow ''rotational resonance'' condition and to reduce the sensitivity of the polarization transfer to experimental settings (*12*). The main application of rotational resonance is to determine distances in selectively doubly labeled compounds (*13–16*).

For the observation of total-correlation spectra where the resonances of all coupled spins are connected by cross peaks, other schemes must be employed. One possibility is to reestablish static conditions during the mixing-time of the NMR experiment through a tilt of the sample-rotation axis away from the magic-angle direction (*17–19*). Then, polarization-transfer schemes developed for static samples and reviewed in Ref. (*17*) can be employed. While this approach leads to full recovery of the dipolar interaction and very broadband recoupling can be achieved, it requires specialized equipment and may be difficult to combine with high spinning speeds. Alternatively, the sample rotation axis can remain fixed at the magic angle and partial dipolar recoupling can be obtained by the application of RF pulses. Several sequences have been proposed that lead to a nonvanishing

1090-7807/97 $25.00

dipolar interaction over one or a few rotor periods (*20–31*). Some of the pulse schemes (*20, 22, 25, 26, 28, 29*) lead to an effective double-quantum dipolar operator $S_k^+ S_l^+ + S_k^- S_l^-$ while others contain the usual zero-quantum term ($S_k^+ S_l^- + S_k^- S_l^+$) found in the high-field dipolar interaction in static samples (*21, 23, 24, 26*). For two-spin systems, both schemes are, in principle, equivalent. The zero-quantum operator preserves the sum polarization of the two spins and leads to an evolution of the difference polarization that is, if a damping term is added, described by a decay of the difference polarization. The double-quantum operator, in contrast, conserves the difference polarization, and an evolution of the sum polarization takes place. For a many-spin system, however, the zero-quantum operator leads to a simpler behavior. A simple constant of the motion, the total polarization of all spins, remains conserved and the polarization is just redistributed over the different spins involved. The process can be described by a kinetic matrix where the column sums vanish, expressing the conservation law. For double-quantum operators, no simple constants of the motion exist, differential polarization-transfer (instead of net polarization transfer) takes place, and the quantitative interpretation of the spectra becomes more difficult. We therefore concentrate, in this paper, on zero-quantum transfer, using the R/L (''rotating/laboratory'' frame) driven transfer principle (*24, 26*).

The cross-peak intensity from total correlation spectra can be interpreted in terms of internuclear distances only if unwanted spectral contributions to the polarization transfer efficiency can be eliminated and the cross-peak intensity is independent of chemical shifts as in the liquid-state nuclear Overhauser enhancement spectroscopy. To characterize the cross-peak intensities, we investigate in detail the properties of the R/L pulse sequences. We will employ average Hamiltonian theory (AHT) (*32*) to first order which, in the present context, is simpler to handle than Floquet methods. We keep, however, in mind that there are limitations to the AHT approach that have already been discussed in the literature (*33*) and complement the AHT treatment by numerically evaluated effective average Hamiltonians and calculations of the trajectory of the density operator.

The paper is organized as follows: The model Hamiltonian, which includes the interaction of the observed *S* spins (e.g., ^{13}C) with abundant but not observed spins, e.g., protons, is described in Section 2. In Section 3, a detailed description of the R/L pulse sequences, including higher order AHT terms, is given and the design principles are highlighted. The conclusions for practical applications, distilled out of the calculations and simulations of Section 3, are presented in Section 4. In the experimental part (Section 5), applications to a multispin system, uniformly ^{13}C labeled arginine, are discussed and cross-peak buildup curves are presented.

2. THE MODEL HAMILTONIAN

We consider a spin system of *N S* spins (e.g., ^{13}C) coupled to *M I* spins (e.g., ^{1}H) under magic-angle sample spinning and subjected to RF irradiation. We partition the ''internal'' rotating-frame Hamiltonian,

$$H_{\text{int}}(t) = H_S(t) + H_I(t) + H_{IS}(t), \qquad [1]$$

into contributions containing only *S* spin terms, only *I* spin terms, and heteronuclear *IS* terms, respectively.

$H_S(t)$ and $H_I(t)$ both contain the same four terms, namely the isotropic chemicals shift (CS), the chemical-shift anisotropy (CSA), the dipolar coupling (D), and the isotropic scalar coupling (J)

$$H_\alpha(t) = H_{\alpha,\text{CS}} + H_{\alpha,\text{CSA}}(t) + H_{\alpha,D}(t) + H_{\alpha,J}, \qquad [2]$$

where α is S or I. The heteronuclear interaction contains dipolar and scalar coupling contributions

$$H_{IS}(t) = H_{IS,D}(t) + H_{IS,J}. \qquad [3]$$

The time dependence in Eqs. [2] and [3] is a consequence of MAS, and the time-dependent coefficients contained in these Hamiltonians, $k(t)$, can be expanded in a Fourier series with four nonzero components only:

$$k(t) = \sum_{n=\pm 2,\pm 1} k_n e^{in\omega_R t}. \qquad [4]$$

Here, ω_R denotes the circular frequency of the sample rotation. The coefficient k_0 and coefficients with an index of three or higher vanish because all time-dependent spatial interactions are described by traceless second-rank tensors (*34*). In a more explicit form, the interactions contained in the internal Hamiltonian considered take the form

$$H_{I,CS} = \sum_{k=1}^{M} \aleph_k I_{kz}$$

$$H_{S,CS} = \sum_{k=1}^{N} \Omega_k S_{kz}$$

$$H_{I,CSA}(t) = \sum_{k=1}^{M} \sum_{n=\pm 2,\pm 1} e_n^{(k)} e^{in\omega_R t} I_{kz}$$

$$H_{S,CSA}(t) = \sum_{k=1}^{N} \sum_{n=\pm 2,\pm 1} c_n^{(k)} e^{in\omega_R t} S_{kz}$$

$$H_{S,D}(t) = \sum_{k<l} \sum_{n=\pm 2,\pm 1} b_n^{(k,l)} e^{in\omega_R t} \times \left[2S_{kz}S_{lz} - \frac{1}{2}(S_k^+ S_l^- + S_k^- S_l^+) \right]$$

$$H_{I,D}(t) = \sum_{k<l} \sum_{n=\pm 2,\pm 1} a_n^{(k,l)} e^{in\omega_R t} \times \left[2I_{kz}I_{lz} - \frac{1}{2}(I_k^+ I_l^- + I_k^- I_l^+) \right]$$

$$H_{IS,D}(t) = \sum_{k<l} \sum_{n=\pm 2,\pm 1} 2d_n^{(k,l)} e^{in\omega_R t} [I_{kz}S_{lz}]$$

$$H_{I,J} = 2\pi \sum_{k<l} J_{kl}^I \mathbf{I}_k \mathbf{I}_l$$

$$H_{S,J} = 2\pi \sum_{k<l} J_{kl}^S \mathbf{S}_k \mathbf{S}_l$$

$$H_{IS,J} = 2\pi \sum_{k<l} J_{kl}^{IS} I_{kz} S_{lz}. \quad [5]$$

The isotropic chemical shifts of the I and S spins are denoted by $\aleph_k$ and Ω_k, respectively. They are measured with respect to the two RF carrier frequencies. The Fourier components of the CSA tensors are, for the S spins, given by

$$c_{\pm 1}^{(k)} = \pm \frac{\gamma_k B_0}{3\sqrt{2}} \delta_k \sin(\theta_k) e^{\pm i\varphi_k} \times [\pm(3 - \eta_k \cos(2\chi_k))\cos(\theta_k) + i\eta_k \sin(2\chi_k)]$$

$$c_{\pm 2}^{(k)} = \frac{\gamma_k B_0}{36} \delta_k e^{\pm 2i\varphi_k} \times \left[\frac{3}{2}\sin^2(\theta_k) + \frac{\eta_k}{2}(1 + \cos^2(\theta_k))\cos(2\chi_k) \mp i\eta_k \cos(\theta_k)\sin(2\chi_k) \right] \quad [6]$$

and depend on three angles φ_k, θ_k, χ_k that describe the time-independent Euler transformation from the rotor-fixed axes system to the principal axis system of the CSA tensor of spin k. The CSA components $e_n^{(k)}$ of the I spins can be defined analogously.

The Fourier components of the homonuclear and heteronuclear dipolar coupling frequencies $b_n^{(k,l)}$, $a_n^{(k,l)}$ and $d_n^{(k,l)}$ are all of the same general form. Here we give only the expressions for $b_n^{(k,l)}$

$$b_{\pm 1}^{(k,l)} = -\frac{b^{(k,l)}}{2\sqrt{2}} \sin(2\theta^{k,l}) e^{\pm i\varphi^{k,l}}$$

$$b_{\pm 2}^{(k,l)} = \frac{b^{(k,l)}}{4} \sin^2(\theta^{k,l}) e^{\pm 2i\varphi^{k,l}} \quad [7]$$

with the dipolar coupling constant

$$b^{(k,l)} = -\mu_0 \gamma_k \gamma_l \hbar / 4\pi r_{kl}^3, \quad [8]$$

where $\theta^{k,l}$ and $\varphi^{k,l}$ are the polar angles that describe the direction of the internuclear vector $\mathbf{r}_{IS}$ in a MAS rotor-fixed coordinate system with the z axis along the sample rotation axis.

J_{kl}^I, J_{kl}^S, and J_{kl}^{IS} denote the isotropic scalar coupling constants. Anisotropic contributions to the J coupling have been neglected and may be incorporated into $b_n^{(k,l)}$, $a_n^{(k,l)}$, and $d_n^{(k,l)}$, respectively.

The total Hamiltonian consists of the internal Hamiltonian and the interaction with the (in general time-dependent) RF fields applied to the two spin species

$$H = H_{\text{int}} + H_{\text{RF}}, \quad [9]$$

with

$$H_{\text{RF}} = H_{I,\text{RF}}(t) + H_{S,\text{RF}}(t) \quad [10]$$

and

$$H_{I,\text{RF}}(t) = \sum_{k=1}^{M} \omega_{1,I}(t)[I_{kx}\cos(\phi_I(t)) + I_{ky}\sin(\phi_I(t))]$$

$$H_{S,\text{RF}}(t) = \sum_{k=1}^{N} \omega_{1,S}(t)[S_{kx}\cos(\phi_S(t)) + S_{ky}\sin(\phi_S(t))], \quad [11]$$

where RF amplitudes $\omega_1(t)$ and phases $\phi(t)$ are under control of the experimentalist and are assumed to be periodically time-dependent.

The evolution of the spin system is described by the propagator

$$U(t) = T \exp\left\{ -i \int_0^t H(t')dt' \right\}, \quad [12]$$

where T denotes the Dyson time-ordering operator. If the cycle time of the time dependences contained in H_{int} and H_{RF} are equal or if a small common denominator exists, an AHT–Ansatz can be made

$$U(t) = T \exp\left\{ -i \int_0^t H_{\text{RF}}(t')dt' \right\} \times T \exp\left\{ -i \int_0^t \tilde{H}_{\text{int}}(t')dt' \right\} = U_{\text{RF}}(t) U_{\text{int}}(t), \quad [13]$$

with

$$\tilde{H}_{\text{int}}(t) = U_{\text{RF}}^{-1}(t) H_{\text{int}}(t) U_{\text{RF}}(t). \quad [14]$$

Equation [14] expresses the internal Hamiltonian of Eq. [1] in the interaction representation of the RF pulse

scheme. Provided that the pulse sequence is periodic with the rotor period τ_c as well as cyclic, $U_{RF}(\tau_c) = 1$, the Magnus expansion (*32, 34, 35*) can be used to describe the time evolution by an effective, time-independent Hamiltonian $\bar{H}$ that would produce after each full cycle the same evolution as $\tilde{H}_{int}(t)$

$$U(n\tau_c) = \exp(-in\bar{H}\tau_c). \quad [15]$$

$\bar{H}$ can be approximated by the truncated series expansion

$$\bar{H} \approx \sum_{n=0}^{N} \bar{H}^{(n)}, \quad [16]$$

where the first terms are given by

$$\bar{H}^{(0)} = \frac{1}{\tau_c}\int_0^{\tau_c} \tilde{H}(t)dt, \quad [17]$$

and

$$\bar{H}^{(1)} = \frac{-i}{2\tau_c}\int_0^{\tau_c} dt_2 \int_0^{t_2} [\tilde{H}(t_1), \tilde{H}(t_2)]dt_1. \quad [18]$$

To evaluate the off-resonance performance of a particular pulse scheme beyond the limits of a first-order AHT treatment, we will resort to numerical simulations. Then, the effective Hamiltonian can be evaluated from the logarithmic relation

$$\bar{H} = -\frac{i}{\tau_c}\ln U(\tau_c), \quad [19]$$

where the propagator over the entire cycle time τ_c is readily approximated as the ordered product over the propagators from small time steps where the Hamiltonian can be assumed to be time independent and within which the propagator can be evaluated in the standard way:

$$U(\tau_c) = \prod_k U_k(t_k). \quad [20]$$

For pulse sequences with a nonvanishing RF field (integrated over one cycle time), the procedure described in Ref. (*17*) has been employed to avoid problems with the nonuniqueness of the logarithm found in Eq. [19].

3. R/L PULSE SCHEMES

It is the aim of the recoupling pulse sequences described here to obtain a time-evolution of the S spin polarization that can be described by an effective Hamiltonian consisting only of the homonuclear dipolar contribution $\bar{H} = \alpha H_{S,D}$ with $|\alpha|$ as large as possible. The pulse sequences discussed here are based on the R/L driven polarization-transfer scheme (*24, 26*) that exploits the different sign of the dipolar Hamiltonian in the laboratory and rotating frames, respectively. This behavior has also been exploited for dipolar coherence echoes (''magic echoes'') (*36–38*) and polarization echoes (*39*). The sign inversion of the spin part of the Hamiltonian, if applied in synchronicity with the sample rotation, leads to a recovery of the dipolar interactions averaged by fast MAS alone (*40, 41*).

3.A. The Basic Pulse Sequence

The basic principle behind all the pulse sequences discussed here can most easily be illustrated for the simple pulse scheme shown in Fig. 1a. For the moment we assume that all interactions, except of the homonuclear dipolar interaction, vanish and that $\omega_{1,S} \to \infty$ (limit of strong RF fields). The $(\pi/2)_y$ pulses are treated in the delta-pulse limit. We use a tilted coordinate system that is related to the usual rotating frame by a $\pi/2$ rotation around the y axis such that the new z axis points along the RF field direction. Then the interaction-frame Hamiltonian, averaged over the ''R'' part of the pulse sequence, is given by

$$\langle H_{S,D}\rangle_R = \sum_{k<l} \frac{-b^{(k,l)}}{\sqrt{2}\pi} \sin(2\theta^{kl})\sin\varphi^{kl} \times \left[2S_{kz}S_{lz} - \frac{1}{2}(S_k^+S_l^- + S_k^-S_l^+)\right], \quad [21]$$

the average over the ''L'' part by:

$$\langle H_{S,D}\rangle_L = \sum_{k<l} \frac{-2b^{(k,l)}}{\sqrt{2}\pi} \sin(2\theta^{kl})\sin\varphi^{kl} \times \left[2S_{kz}S_{lz} - \frac{1}{2}(S_k^+S_l^- + S_k^-S_l^+)\right], \quad [22]$$

and the zeroth-order average Hamiltonian of the entire pulse sequence is given by

$$\bar{H}^{(0)}_{S,D} = \sum_{k<l} \frac{-3b^{(k,l)}}{2\sqrt{2}\pi} \sin(2\theta^{(kl)})\sin\varphi^{kl} \times \left[2S_{kz}S_{lz} - \frac{1}{2}(S_k^+S_l^- + S_k^-S_l^+)\right]. \quad [23]$$

Equation [23] is the desired Hamiltonian with $b^{(k,l)}$ as defined in Eq. [8]. Note that the Hamiltonian of Eq. [23] is exact ($\bar{H} = \bar{H}^{(0)}_{S,D}$) for a two-spin system with dipolar interaction only. For more than two spins, higher order average Hamiltonian terms can appear. Because the spinning frequency is usually large compared to the

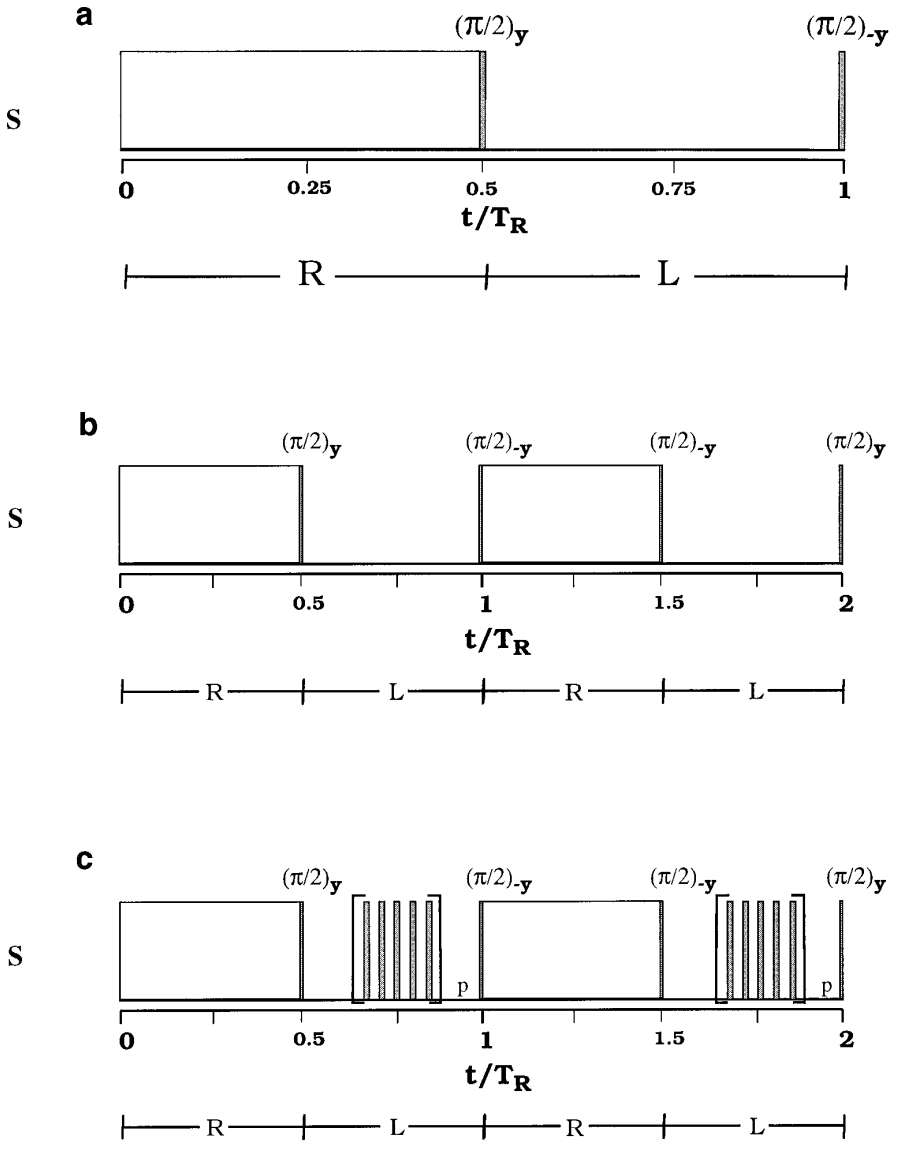

FIG. 1. (a) Basic R/L scheme applied to the *S* spins, consisting of a CW (rotating frame, ''R'') spin lock and, enclosed by two 90° pulses of opposite phase, a laboratory frame part (''L'') covering the first and second half of a rotor period, respectively. (b) R/L supercycle where in two consecutive MAS periods the RF phase of both 90° *y* pulses is inverted, and (c) where additional π refocusing pulses are introduced in the L part.

magnitude of the *S*-spin homonuclear dipolar interactions ($\omega_R \gg d^{(kl)}$), these can be neglected in good approximation.

The orientational dependence of the dipolar interaction under the R/L sequence (Eq. [23]) is characterized by two Euler angles (θ^{kl} and φ^{kl}). The resulting powder pattern has a similar form and width as found for the DRAMA, MELODRAMA, or DRAWS with the highest intensity in the center of the pattern. The double-quantum sequences HORROR and C7 show a pattern that depends on a single Euler angle (θ^{kl}) and have a (more favorable) powder pattern with the highest intensities at the extreme frequencies. Correspondingly, these two double-quantum sequences show a more pronounced oscillation of the transferred magnetization as a function of transfer time. For a zero-quantum sequence, such a behavior has not been realized to date.

It is an interesting property of the basic pulse sequence that it leads, if the L part is applied before the R part (L/R), to the same Hamiltonian as the R/L sequence, except for a sign change. Therefore, consecutive application of an R/L and a L/R pulse sequence lead, for a super cycle (SC) covering two rotor periods, to a complete dipolar echo with $\bar{H}_{S,D}^{(0,SC)} = 0$. This behavior was first pointed out and applied to coherence- and polarization-echo formation by Tomaselli and Ernst (*42*, *43*).

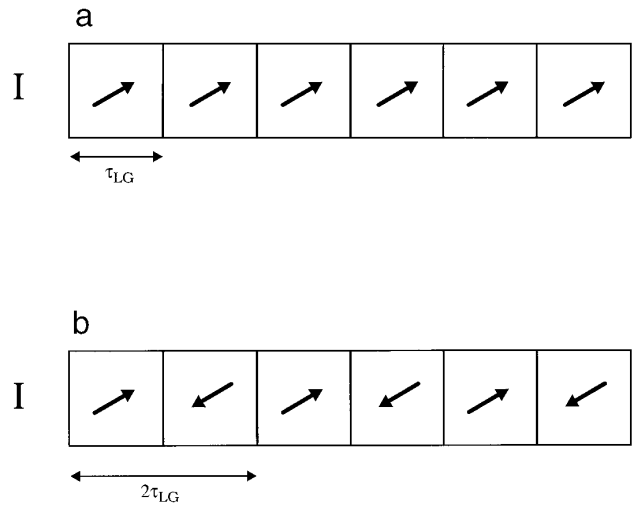

FIG. 2. (a) Lee–Goldburg homonuclear decoupling (*45*) applied to the *I* spins which are irradiated by an off-resonance RF field such that the effective field direction (indicated by the arrow) is tilted by the magic angle with respect to the static magnetic field. (b) Frequency switched (FS) version of the basic LG decoupling method introduced by Bielecki *et al.* (*47, 48*) where after completion of a 2π rotation (or a multiple of it) around the effective field axis (represented by one block), the sign of the phase and frequency offset are simultaneously inverted (consecutive block).

3.B. Chemical-Shift and Heteronuclear-Coupling Compensated Pulse Schemes

The simple pulse sequence of Fig. 1a used to illustrate the principle of the R/L pulse sequences is only applicable if, besides the homonuclear dipolar interactions, no other interactions are present. The other interactions as listed in Eq. [5] do also lead to strong and unwanted contributions to the zeroth-order average Hamiltonian of the basic pulse sequence. We aim, in the following, at a pulse scheme that eliminates, at least to zeroth-order AHT, all interactions except $\bar{H}^{(0)}_{S,D}$.

Often, the dipolar coupling to the *I* spins $H_{IS,D}$ is the most problematic term to remove from the effective *S* spin Hamiltonian because the *I* spins are strongly coupled amongst themselves through $H_{I,D}(t)$. For organic solids, *I*-spin (proton) homonuclear dipole interactions are typically comparable to or larger than technically possible MAS frequencies. Furthermore, $H_{I,D}(t)$ behaves heterogeneously under sample rotation (*44*) with $[H_{I,D}(t_1), H_{I,D}(t_2)] \neq 0$ even during time intervals with a time-independent RF Hamiltonian and renders the heteronuclear dipolar interaction also homogeneous and difficult to remove. It is therefore essential to average this large term, $H_{I,D}(t)$, by a cyclic RF perturbation $H_{I,\mathrm{RF}}(t)$ with a cycle time as short as possible and shorter than the inverse MAS frequency. The pulse sequences of Fig. 1 can, to this purpose, be combined with one of the Lee–Goldburg homonuclear dipolar decoupling schemes given in Fig. 2. In Fig. 2a the protons are continuously irradiated by an RF field applied off-resonance such that the angle θ_k between the effective field and the static magnetic field equals the magic angle (*45*):

$$\tan\theta_k = \frac{\omega_{1,I}}{\aleph_k} = \sqrt{2} \text{ for all } k. \qquad [24]$$

Rigorously, this can only be fulfilled if all *I* spins have the same isotropic chemical shift ($\aleph_k = \aleph$ and $\theta_k = \theta = \arctan\sqrt{2}$ for all k) and if the proton CSA vanishes. For strong RF fields, condition [24] can, however, be sufficiently well fulfilled. Because $|\omega_{1,I}| \gg |a^{(k,l)}|$ for all spin pairs (k, l), the *I* spins are quantized along the effective field direction, and it is beneficial to describe the *I* spin interactions in a tilted frame with the new *z* axis, denoted by *Z*, tilted by θ around the *y* axis. The *I* spin operators in the tilted frame are given by

$$\begin{aligned} I_{kZ} &= I_{kz}\cos(\theta) + I_{kx}\sin(\theta), \\ I_{kX} &= I_{kx}\cos(\theta) - I_{kz}\sin(\theta), \text{ and} \\ I_{kY} &= I_{ky}. \end{aligned} \qquad [25]$$

Hence, the homonuclear dipolar contribution of the *I* spins (as given in Eq. [5]) reads, in the tilted frame, as

$$H_{I,D}(t) = \sum_{k<l} \sum_{n=\pm2,\pm1} a_n^{(k,l)} e^{in\omega_R t} \Big[\sum_{m=-2}^{2} \lambda_{2,m}(\theta) T_{2,m}(k,l) \Big], \qquad [26]$$

where

$$\begin{aligned} T_{2,0}(k,l) &= \tfrac{1}{\sqrt{6}}[2I_{kZ}I_{lZ} - \tfrac{1}{2}(I_k^+ I_l^- + I_k^- I_l^+)] \\ T_{2,\pm1}(k,l) &= \mp\tfrac{1}{2}[I_k^\pm I_{lZ} + I_{kZ} I_l^\pm] \\ T_{2,\pm2}(k,l) &= \tfrac{1}{2} I_k^\pm I_l^\pm \end{aligned} \qquad [27]$$

and

$$\begin{aligned} \lambda_{2,0}(\theta) &= \sqrt{\tfrac{3}{8}}\,(3\cos^2\theta - 1) \\ \lambda_{2,\pm1}(\theta) &= \mp\tfrac{3}{4}\sin(2\theta) \\ \lambda_{2,\pm2}(\theta) &= \tfrac{3}{4}\sin^2(\theta) \end{aligned} \qquad [28]$$

Now, an interaction representation (see Eq. [14]) along the new *z* axis, I_{kZ}, with respect to $\omega_{\mathrm{LG}} = \sqrt{\omega_{1,I}^2 + \aleph^2}$ can be chosen,

$$U_{\mathrm{RF}}(\iota) = \exp[i\omega_{LG} \sum_k I_{kZ}\iota], \qquad [29]$$

to describe the homonuclear dipolar coupling among the I spins in the interaction representation with respect to Lee–Goldburg I spin RF irradiation. The corresponding time variable is denoted by ι to distinguish it from the much slower t time dependence caused by the sample rotation and the S spin multiple-pulse sequence.

Using the commutation relation $[S_{kZ}, T_{2,m}(k, l)] = mT_{2,m}(k, l)$ one finds that

$$\tilde{H}_{I,D}(t, \iota) = \sum_{k<l} \sum_{n=\pm 2,\pm 1} a_n^{(k,l)} e^{in\omega_R t} \times [\sum_{m=-2}^{2} \lambda_{2,m}(\theta)(T_{2,m}(k, l)\exp[im\omega_{LG}\iota])]. \quad [30]$$

Since we assume strong RF fields it is justified to treat the ''slow'' t time dependence introduced through the MAS spinning speed as parametric and apply AHT with respect to ι [46]. The cycle time is then given by $\tau_{LG} = 2\pi/\omega_{LG}$. We find easily the zeroth-order AHT result:

$$\bar{H}_{I,D}^{(0)}(t) = \frac{1}{\tau_{LG}} \left[\int_0^{\tau_{LG}} \tilde{H}_{I,D}(t, \iota')d\iota' \right] = 0. \quad [31]$$

The remaining I spin terms such as the CS, CSA, or the heteronuclear dipolar interaction are linear in the I spin operators. For the CS term one obtains

$$\bar{H}_{I,CS}^{(0)}(t) = \frac{1}{\tau_{LG}} \left[\int_0^{\tau_{LG}} \tilde{H}_{I,CS}(t, \iota')d\iota' \right] = \frac{1}{\sqrt{3}} H_{I,CS}. \quad [32]$$

The CSA terms and the IS coupling terms scale exactly the same as the CS terms because, during the short time period τ_{LG}, the t time dependence is neglected:

$$\bar{H}_{I,CSA}^{(0)}(t) = \frac{1}{\sqrt{3}} H_{I,CSA}(t), \quad [33]$$

$$\bar{H}_{IS,D}^{(0)}(t) = \frac{1}{\sqrt{3}} H_{IS,D}(t), \quad [34]$$

and

$$\bar{H}_{IS,J}^{(0)}(t) = \frac{1}{\sqrt{3}} H_{IS,J}(t). \quad [35]$$

With the decoupling scheme of Fig. 2a we have achieved our first goal, to remove the I spin homonuclear dipole interaction (see Eq. [31]), but have retained the other I spin interactions in a scaled form. These terms will be averaged out at a later stage. It might be possible to suppress first-order AHT terms of the Lee–Goldburg sequence by the application of the frequency-switched LG decoupling scheme of Fig. 2b (*47, 48*). In the frequency-switched version, the resonance offset and the phase of the RF irradiation are inverted in the second period of the supercycle (see Fig. 2b).

Having eliminated the fast ι time dependence by AHT, we apply next a second AHT treatment where we average over one cycle of the ''slow'' t dependence with a cycle time of $\tau_c = 2\pi/\omega_R$ or over one supercycle (Fig. 1b)) with a cycle time of $2\tau_c$. Such a sequential averaging scheme may be applied because the time scales of the two processes are quite different: $\tau_{LG} \ll \tau_c$. However, we still remain in the regime where $\tau_c \ll 1/|\bar{H}_{int}^{(0)}|$.

First, we consider the chemical-shielding terms on the S spins, a pure S spin quantity not influenced by the I spin irradiation. During the R part of the pulse sequence, the presence of the S spin RF field suppresses all zero-order CS or CSA contributions, but the CS as well as CSA contributions remaining in the L period lead to

$$\bar{H}_{S,CS}^{(0)} = \frac{1}{2} \sum_{k=1}^{N} \Omega_k S_{kz} \quad [36]$$

and

$$\bar{H}_{S,CSA}^{(0)} = \sum_k \frac{2\gamma_k B_0}{3\pi\sqrt{2}} \delta_k \sin\theta_k([\sin\varphi_k(3 - \eta_k\cos(2\chi_k))\cos\theta_k + \cos\varphi_k\eta_k\sin(2\chi_k)])S_{kz}. \quad [37]$$

Note that again the tilted frame for the S spins (introduced in the preceding subsection) is used. The introduction of one π pulse (e.g., in the middle of the L part) is sufficient to suppress the zeroth-order isotropic chemical-shift contributions. As shown previously (*26*), the CSA contributions decrease with an increasing number of refocusing π pulses and vanish for an infinite number of refocusing pulses (Fig. 1c). Then one obtains, as desired,

$$\bar{H}_{S,CS}^{(0)} = 0 \quad \text{and} \quad \bar{H}_{S,CSA}^{(0)} = 0. \quad [38]$$

For a finite number r of symmetrically arranged refocusing pulses the CSA interaction is scaled according to

$$\bar{H}_{S,CSA}^{(0)} = \sum_k \left(i(c_2^{(k)} - c_{-2}^{(k)})\delta_{r1} + \sum_{p=1,2} \sum_{q=r+2}^{2r+1} \frac{(-1)^{p+q}}{p} \times [c_{-p}^{(k)} + c_p^{(k)}]\sin\left(\frac{pq\pi}{r+1}\right)\right) S_{kz}, \quad [39]$$

where the $c_n^{(k)}$ are given in Eq. [6].

The CSA terms that remain after the application of the refocusing pulses are removed after the super cycle of Fig. 1c and we obtain

$$\bar{H}_{S,\mathrm{CSA}}^{(0,\mathrm{SC})} = \bar{H}_{S,\mathrm{CS}}^{(0,\mathrm{SC})} = 0. \qquad [40]$$

It should be noted that the result of Eq. [40] is also obtained after application of the supercycle alone, without that π refocusing pulses (Fig. 1b). However, because the averaging appears over a much larger time interval, it is less effective, meaning that higher order AHT terms play a more important role.

We also must investigate the behavior of the (scaled) IS heteronuclear coupling terms. To zeroth order they behave as the CSA terms. Depending on the setting of the amplitudes of the I and S spin RF fields, heteronuclear cross-polarization effects may however take place by accidentally matching the effective field ω_{LG} with the components of the amplitude-modulated S spin irradiation. These effects have been discussed in detail by Hediger *et al.* (*49*) and can usually be neglected under the conditions discussed in this paper.

We therefore obtain for the super cycle as desired:

$$\bar{H}_{IS,D}^{(0,0,\mathrm{SC})} = 0 \qquad [41]$$

and

$$\bar{H}_{IS,J}^{(0,0,\mathrm{SC})} = 0. \qquad [42]$$

Here, the superscript (0, 0) denotes that with respect to both averaging procedures, zeroth-order AHT was applied.

Thus, all unwanted terms of Eq. [5] vanish over the supercycle of Fig. 1c and we obtain

$$\bar{H}^{(0,0)} = \bar{H}_{S,D}^{(0)} + \bar{H}_{S,J}^{(0)} + \bar{H}_{I,J}^{(0)}. \qquad [43]$$

The desired term $\bar{H}_{S,D}^{(0)}$ is given in Eq. [23]. The term $\bar{H}_{I,J}^{(0)}$ commutes with the two other terms and may be omitted. The homonuclear scalar couplings are usually one or two orders of magnitude smaller than their corresponding dipolar counterparts such that we obtain

$$\bar{H}^{(0,0)} \approx \bar{H}_{S,D}^{(0)} \qquad [44]$$

which is our desired effective Hamiltonian.

3.C. The Case of Finite RF Field Strength

Finite RF field strength in the R part only. Next, we consider the case when an RF field of finite strength is applied during the R part. As a simple example, we assume that during the R part, a $s\cdot\pi$ pulse rotation angle (where s is an integer) is completed (see Fig. 3a). This requires that

$$\frac{\omega_{1,S}}{\omega_{\mathrm{R}}} = s. \qquad [45]$$

In order to simplify the problem we still treat the $\pi/2$ pulse before and after the L part in the delta-pulse limit (Fig. 3a). The zeroth-order dipolar contributions are then (for $s > 1$) given by

$$\begin{aligned}\bar{H}_{S,D}^{(0)} = \sum_{k<l} \frac{-3b^{(k,l)}}{2\sqrt{2}\pi} \sin(2\theta^{(kl)}) \\ \times \Big\{ \sin\varphi^{(kl)} \Big[2S_{kz}S_{lz} - \frac{1}{2}(S_k^+S_l^- + S_k^-S_l^+) \\ + \epsilon(S_k^+S_l^+ + S_k^-S_l^-) \Big] \\ - \cos\varphi^{(kl)}\epsilon'(S_{kx}S_{ly} + S_{ky}S_{lx}) \Big\}\end{aligned} \qquad [46]$$

with $\epsilon = 1/(16s^2 - 4)$ and $\epsilon' = 4s/(12s^2 - 3)$. In the limit of strong RF irradiation, $s \to \infty$, we find $\epsilon = \epsilon' = 0$ and Eq. [46] reduces to Eq. [23]. In all practical applications s is large enough to neglect these finite RF modifications to the dipolar Hamiltonian.

For the zeroth-order AH contribution of the isotropic chemical shift term in the R part, we obtain (*19*)

$$\begin{aligned}\bar{H}_{S,CS}^{(0)} = \frac{a}{2\tau_c}\left(\frac{\Omega_1}{\omega_1}S_{1x} + \frac{\Omega_2}{\omega_1}S_{2x}\right) \\ + \frac{b}{2\tau_c}\left(\frac{\Omega_1}{\omega_1}S_{1y} + \frac{\Omega_2}{\omega_1}S_{2y}\right).\end{aligned} \qquad [47]$$

Using Eq. [221] of Ref. (*17*), we find $a = \sin\alpha$ and $b = \cos\alpha - 1$ where α is the rotation angle completed during the R period. We have assumed that s is integer and, with Eq. [45] we obtain

$$\bar{H}_{S,\mathrm{CS}}^{(0)} = 0. \qquad [48]$$

For the heteronuclear-dipolar and chemical-shielding interactions only minor modifications of the zeroth-order AHT terms obtained under infinite field strength are observed. They are given in Appendix A and can be neglected because they are on the same order of magnitude as the ϵ discussed above.

Up to now, we have only considered zeroth-order AH contributions. For large chemical shifts, first-order terms may also become important (Eq. [18]). The ''auto'' terms (CS × CS) of the isotropic chemical shift lead to

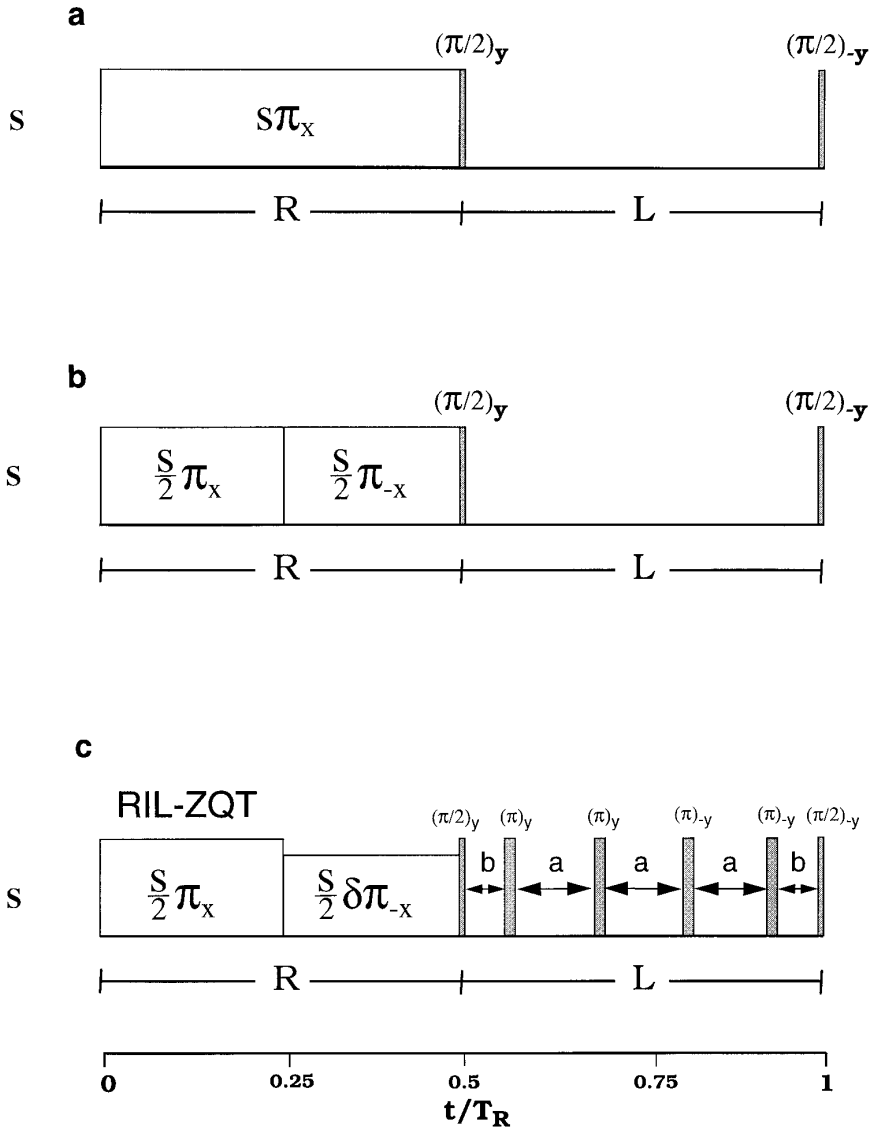

FIG. 3. (a) Basic R/L scheme applied to the *S* spin with finite RF field strength in the R part. An effective flip angle of $s\pi$ is assumed. (b) an additional phase inversion is applied in the middle of the R interval. (c) Model RIL-ZQT scheme that incorporates phase switching in the R part and refocusing π pulses during the L interval. In addition, an amplitude attenuation δ is introduced in the second quarter of one rotor period. The time intervals *a* and *b* are defined in the text.

$$\bar{H}^{(1)}_{S,\mathrm{CS}\times\mathrm{CS}} = \frac{1}{4}\sum_{k=1}^{N}\frac{\Omega_k^2}{\omega_{1,S}}S_{kz}. \qquad [49]$$

An improved offset dependence can be achieved, if a phase inversion is used in the middle of the R part (Fig. 3b). The zeroth-order AH dipolar term is—except for the small terms proportional to ϵ—invariant under this phase inversion if we assume that *s* is not only an integer but also even. The first-order auto term of Eq. [49] now also vanishes:

$$\bar{H}^{(1,\mathrm{SC})}_{S,\mathrm{CS}\times\mathrm{CS}} = 0. \qquad [50]$$

Thus, we can conclude that an improved offset compensation under finite RF amplitude conditions can be achieved if a phase inversion such as shown in Fig. 3b is incorporated into the R part. We will use—as in Ref. (*26*)—the acronym RIL-ZQT for ''rotating inverse-laboratory zero-quantum transfer'' for the offset-compensated R/L scheme.

Finite RF field strength in the R and L parts. The general AHT analysis of the entire R/L pulse sequence under finite RF strength conditions can become rather complex. To discuss the principles we replace the pulse sequence by a simpler model sequence and consider a spin system of two *S* spins only. The simplified pulse scheme uses no phase inver-

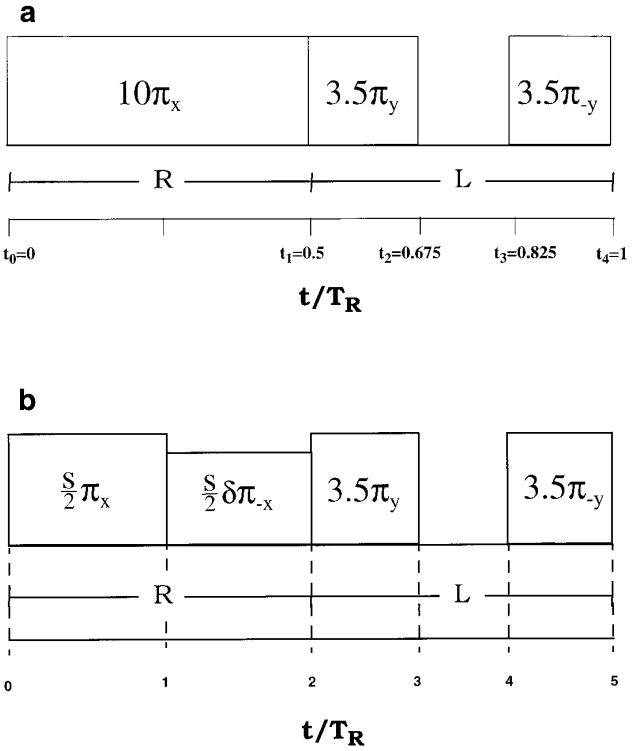

FIG. 4. (a) Simplified R/L scheme with substantial RF irradiation during the laboratory frame (L) part. Only a time interval with a length equivalent to a 3π pulse remains RF free. In (b), an additional amplitude attenuation δ during the time interval [1,2] is introduced. The numbering of the indicated intervals corresponds to the notation used in the text.

sion in the R part and all π pulses are moved toward the beginning or end of the L period. This does not influence the zeroth-order terms but simplifies the first-order terms. The resulting simplified sequence is shown in Fig. 4a. and consists, for the case of six refocusing pulses and $s = 10$, of an L period with two pulses of length 3.5π separated by a free evolution period with a length that corresponds to an 3π pulse. For brevity, we will use in the following the notation $b = b^{(1,2)}/\sqrt{2}$ *and omit all S* indices. The zeroth-order AH, in the absence of CSA terms, consists then of two nonzero terms:

$$\bar{H}^{(0)} = \bar{H}_D^{(0)} + \bar{H}_{\mathrm{CS}}^{(0)}. \qquad [51]$$

The residual chemical-shift contributions are given by

$$\bar{H}_{\mathrm{CS}}^{(0)} = \frac{1}{10 \cdot 2\pi}(\Omega_1((3\pi - 2)S_{1z} - 2S_{1x}) + \Omega_2((3\pi - 2)S_{2,z} - 2S_{2,x})), \qquad [52]$$

and the dipolar contribution can be described by a superposition of zero-, single-, and double-quantum transition operators:

$$\begin{aligned}\bar{H}_D^{(0)} = {} & a^{(0)}(\theta, \varphi)\frac{(S_1^+S_2^- + S_1^-S_2^+)}{2} \\ & + a^{(2)}(\theta, \varphi)\frac{(S_1^+S_2^+ + S_1^-S_2^-)}{2} \\ & + 2a^{(z)}(\theta, \varphi)S_{1z}S_{2z} \\ & + a^{(1,x)}(\theta, \varphi)(S_{1x}S_{2z} + S_{1z}S_{2x}) \\ & + a^{(1,y)}(\theta, \varphi)(S_{1x}S_{2y} + S_{1y}S_{2x}) \qquad [53]\end{aligned}$$

with the coefficients given in Appendix B.

Equation [53] describes the resulting dipolar contribution under the influence of the pulse scheme of Fig. 4a. Under *infinite* RF conditions only two terms were found to contribute (see Eq. [23])

$$a^{(0)} = \frac{3}{2\pi} b \sin(2\theta)\sin(\varphi)$$

$$a^{(z)} = -\frac{3}{2\pi} b \sin(2\theta)\sin(\varphi). \qquad [54]$$

The first term represents the coefficient of the zero-quantum transfer (ZQT) element that actually leads to the desired dipolar recoupling. The relatively small single-quantum terms found in Eq. [B.1] as a result of the finite-strength RF contributions during the R and L part scale inversely proportional to s and do not contribute substantially to the Hamiltonian for $s > 5$. A comparison of Eq. [B.1] and Eq. [54] reveals, however, that due to the presence of finite RF contributions in the L part, a substantial part of the zero-quantum element has been converted into a double-quantum term.

For the supercycle of Fig. 1c the contributions of $\bar{H}_{\mathrm{CS}}^{(0)}$ along I_z and all single-quantum transition terms of Eq. [53] vanish. Unchanged are the zero- and double-quantum elements of the zeroth-order result in Eq. [53].

For our (reduced) problem of a homonuclear two-spin system under MAS the first-order AH is given by three contributions if the CSA interaction is neglected:

$$\bar{H}^{(1)} = \bar{H}_{\mathrm{CS}\times\mathrm{CS}}^{(1)} + \bar{H}_{\mathrm{CS}\times D}^{(1)} + \bar{H}_{D\times D}^{(1)}. \qquad [55]$$

It should be noted that, because we treat the situation with finite RF fields, auto terms like $(D \times D)$ do arise even in an isolated two-spin system. For the pulse sequence of Fig. 4a we find that

$$\bar{H}^{(1)}_{\mathrm{CS}\times\mathrm{CS}} = \frac{1}{4}\left(\frac{\Omega_1^2}{\omega_{1,S}}\left(S_{1z} + \frac{1}{5\pi}S_{1y}\right) + \frac{\Omega_2^2}{\omega_{1,S}}\left(S_{2z} + \frac{1}{5\pi}S_{2y}\right)\right)$$

$$\bar{H}^{(1)}_{\mathrm{CS}\times D} = \tilde{b}\,\frac{(\Omega_1 + \Omega_2)}{2\omega_{1,S}}\,(S_1^+S_2^+ + S_1^-S_2^-) + \frac{b}{\omega_{1,S}}\sum_{\substack{\alpha=x,y,z\\ \alpha\neq\beta}} 2A_{\alpha,\beta}S_{1\alpha}S_{2\beta}$$

$$\bar{H}^{(1)}_{D\times D} = \frac{b^2}{\omega_{1,S}}\sum_{\gamma=x,y,z} B_\gamma(S_{1\gamma} + S_{2\gamma}) \qquad [56]$$

with the effective dipolar coupling $\tilde{b} \approx -2b(0.119\cos\varphi + 0.011\sin\varphi)\sin(2\theta)$. In Eq. [56] we have separated the different contributions arising from auto terms of the chemical shift and the dipolar coupling and cross terms between the dipolar and chemical-shift interactions. The coefficients $A_{\alpha,\beta}$ and B_γ are given in Appendix C. Of particular importance is the flop–flop term contained in $\bar{H}^{(1)}_{\mathrm{CS}\times D}$ which we will discuss in more detail below.

The polarization transfer $S_{1z} \rightarrow S_{2z}$ mediated by the average Hamiltonian $\bar{H}^{(0)} + \bar{H}^{(1)}$ of Eqs. [51]–[56] has been calculated for a single crystallite orientation with a dipolar-coupling frequency $b/2\pi = 500$ Hz and vanishing CSA contributions at a spinning speed of $\omega_R/2\pi = 5$ kHz and for an RF field strength of $\omega_{1,S}/2\pi = 50$ kHz. The results, as a function of the contact time, are shown in Fig. 5a for a number of chemical-shift values chosen to be identical for both spins, corresponding to moving the RF carrier frequency. Exact numerical simulations in the framework of the NMR programming environment GAMMA (*50*), are also shown in Fig. 5a. For small chemical shifts Ω_1 and Ω_2, the AHT coincides remarkably well with the exact calculation. Even at $\Omega_1 = \Omega_2 = 0$, they do, however, not fully coincide due to the effects of finite RF that leads to second- and higher order AHT terms neglected in our AHT treatment. At larger chemical-shift values, a remarkable asymmetry of the transfer with respect to an inversion of the sign of the chemical shifts is observed. This effect has also been found in numerical simulations of the offset behavior of the RIL-ZQT sequence (*26*).

Our model-sequence calculation leads us now to an explanation of this effect: the first-order term $\bar{H}^{(1)}_{\mathrm{CS}\times D}$ of Eq. [56] contributes to the double-quantum element of the effective Hamiltonian with a term that is proportional to $\Omega_1 + \Omega_2$ and inversely proportional to $\omega_{1,S}$ and will add or subtract to the zeroth-order double-quantum contribution depending on the relative signs. At an offset of $\Omega_1 = \Omega_2 = 13$ kHz, the first- and zeroth-order double-quantum terms are of comparable size but they add or subtract, respectively, depending on the sign of $\Omega_1 + \Omega_2$. This asymmetry is preserved in the powder average.

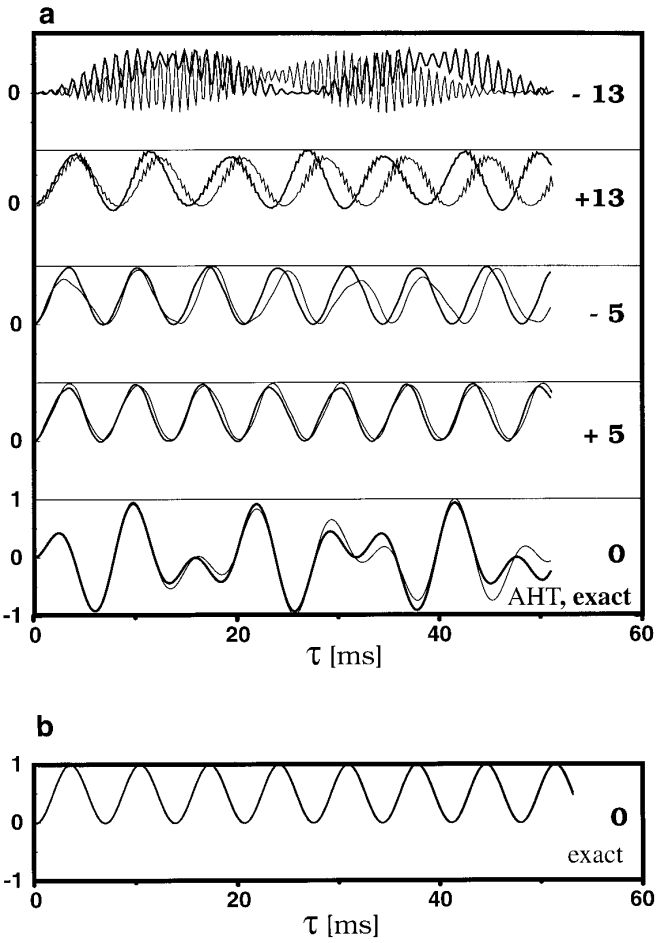

FIG. 5. (a) Transferred polarization to spin 2 after initial polarization on spin 1 only for chemical-shift offsets $\Omega_1 = \Omega_2$ of 0, ±5, ±13 kHz using the pulse scheme of Fig. 4a. An arbitrary single-crystallite orientation with an effective dipolar coupling of 500 Hz and an MAS spinning speed of 5 kHz were assumed. In each column, the results obtained from Eqs. [52]–[56] (first-order AHT) are given by a thin line and the results from an exact simulation by a thicker line. In (b), the exact on-resonance $\Omega_1 = \Omega_2 = 0$ result for the pulse scheme of Fig. 4b is shown using otherwise the same simulation parameters as in (a). All numerical calculations were performed using the NMR programming environment GAMMA (*50*).

The asymmetry is compensated to zeroth order by the supercycle of Figs. 1b and 1c because the inversion of the phase of the y pulses $\phi \rightarrow -\phi$ is equivalent to the replacement $\Omega_1, \Omega_2 \rightarrow -\Omega_1, -\Omega_2$ in Eq. [56]. The prediction that most of the asymmetry is removed by the supercycle is again in accordance with numerical simulations (*26*).

An important implication of finite RF strength is immediately seen from the on-resonance behavior in Fig. 5a where the transferred polarization does *not* sinusoidally oscillate between 0 and 1, corresponding to a net, in-phase polarization transfer, but where an oscillation between 1 and −1 is observed. This can be explained by the appearance of un-

wanted double-quantum terms in Eq. [53]. This contribution can be quenched in the presence of chemical-shift terms (e.g., at $\Omega_1 = \Omega_2 = 5$ kHz). Nevertheless, care must be applied to eliminate this contribution. This will be attempted in the next chapter.

3.D. The Amplitude Attenuation δ

In the preceding chapter we have found that finite RF field strength leads to additional double-quantum contributions to the effective Hamiltonian that may strongly disturb the net polarization transfer occurring under an effective ZQT Hamiltonian and lead to differential transfer and to a decay of the sum polarization in the spin system. In an attempt to quench these terms, we introduce an additional degree of freedom into the pulse sequence and allow for an amplitude attenuation during the R part of the basic R/L scheme (Fig. 3c). It is kept in mind that the introduction of an amplitude attenuation can influence the chemical-shift offset compensation and a compromise will be attempted that combines acceptable shift compensation with a good zero-quantum suppression.

Analytical treatment using the model sequence. For the simplified model sequence analyzed in the previous section, a particularly strong effect of these undesired double-quantum terms was found in the on-resonance case. We are now going to investigate the influence of δ on the effective dipolar Hamiltonian for this model sequence (Fig. 4b). To point out the basic principles, we consider the simplest case and take into account only the dipolar contribution to the total Hamiltonian, $H_{S,D}$. For $\delta \neq 1$, while the Hamiltonian is still periodic with the MAS cycle time, the toggling frame and the usual rotating frame do not coincide with each other any more after one MAS cycle but are rotated with respect to each other by an angle

$$\Theta(\delta, s) = s\frac{\pi}{2}(1 - \delta) \qquad [57]$$

around the x axis and the pulse sequence is not cyclic with the MAS period: $U(\tau_r) \neq 1$. As before, s denotes the ratio of the RF field strength and the MAS frequency. While the noncyclicity of the pulse sequence poses no problems for the performance of the pulse sequence, it renders the AHT treatment more difficult. To explore the effect of an amplitude attenuation we first choose δ such that a flip angle of $\Theta = (l + \frac{1}{2})\pi$ or $\Theta = l\pi$ results, where l denotes an integer. Then, $U(4\tau_r) = 1$ and an AHT treatment is possible if we consider a cycle time of $4\tau_r$. For the five time intervals ($[n, n + 1], n = 0, 1, 2, 3, 4$) of each of the four rotor periods (see Fig. 4) we can now determine the resulting contributions to the zeroth-order dipolar average Hamiltonian $\bar{H}^{(0)}_{[n,n+1]}$. If we abbreviate the necessary integration over the spatial coordinates as

$$B_{k,k+1}(\theta, \varphi) = \int_{t_k}^{t_{k+1}} \sum_{n=-2}^{2} b_n(\theta, \varphi) e^{in\omega_R t} dt, \qquad [58]$$

the average of the dipolar interaction for the [0, 1], [1, 2], and [3, 4] subintervals becomes, for all four subcycles, independent of Θ:

$$\begin{aligned}
\bar{H}^{(0)}_{[0,1]} &= -\tfrac{1}{2}B_{0,1}(\theta,\varphi)[2S_{1z}S_{2z} - \tfrac{1}{2}(S_k^+S_l^- + S_k^-S_l^+)] \\
\bar{H}^{(0)}_{[1,2]} &= -\tfrac{1}{2}B_{1,2}(\theta,\varphi)[2S_{1z}S_{2z} - \tfrac{1}{2}(S_k^+S_l^- + S_k^-S_l^+)] \\
\bar{H}^{(0)}_{[3,4]} &= B_{3,4}(\theta,\varphi)[2S_{1z}S_{2z} - \tfrac{1}{2}(S_k^+S_l^- + S_k^-S_l^+)]. \qquad [59]
\end{aligned}$$

The contribution of the remaining two intervals [2, 3] and [4, 5], in contrast, depend on Θ as well as on the subcycle. For the first and the third rotor period we find for $\Theta = (l + \frac{1}{2})\pi$ or $\Theta = l\pi$:

$$\begin{aligned}
\bar{H}^{(0)}_{[2,3]} &= \bar{H}^{(0)}_{[4,5]} \\
&= -\tfrac{1}{2}B_{4,5}(\theta, \varphi)[2S_{1x}S_{2x} \\
&\quad - \tfrac{1}{2}(S_k^+S_l^- + S_k^-S_l^+)]. \qquad [60]
\end{aligned}$$

This contribution is not of the desired form (proportional to $2S_{1z}S_{2z} - \frac{1}{2}(S_k^+S_l^- + S_k^-S_l^+)$) and gives rise to the discussed double-quantum terms. For the second and the last rotor period (subcycle) we have, for $\Theta = l\pi$, again the result of Eq. [60] but for $\Theta = (l + \frac{1}{2})\pi$, we find that

$$\begin{aligned}
\bar{H}^{(0)}_{[2,3]} &= \bar{H}^{(0)}_{[4,5]} \\
&= -\tfrac{1}{2}B_{4,5}(\theta, \varphi)[2S_{1y}S_{2y} \\
&\quad - \tfrac{1}{2}(S_k^+S_l^- + S_k^-S_l^+)]. \qquad [61]
\end{aligned}$$

Since $S_{1x}S_{2x} + S_{1y}S_{2y} = 1/2(S_k^+S_l^- + S_k^-S_l^+)$ the unwanted DQT contributions vanish if $\Theta = (l + \frac{1}{2})\pi$ and net ZQT transfer can proceed under a Hamiltonian

$$\bar{H}^{(0)}_{S,D} = b_{eff}[2S_{1z}S_{2z} - \tfrac{1}{2}(S_k^+S_l^- + S_k^-S_l^+)] \qquad [62]$$

with $b_{eff} = B_{3,4} - (1/2)B_{0,2} - \frac{1}{2}(B_{2,3} + B_{4,5})$. The resulting polarization transfer to spin 2 is displayed in Fig. 5b) and displays, unlike the case $\delta = 1$, the desired oscillatory zero-quantum polarization transfer. For $\Theta = l\pi$, the unwanted terms remain unattenuated.

The above given arguments are not limited to the case of $\Theta = (l + \frac{1}{2})\pi$. For example, for $\Theta = (l + \frac{1}{3})\pi$ similar arguments could be presented for a AHT cycle time of $6\tau_R$. Any angle $\Theta \neq l\pi$ will lead to an attenuation of the unwanted terms. However, $\Theta = (l + \frac{1}{2})\pi$ is most effective because it requires the shortest cycle time.

Numerical simulations for the RIL sequence. Above we have found analytically that an amplitude attenuation δ can

eliminate the unwanted double-quantum terms, for the simplified model sequence. Standard AHT can, however, only be employed if the toggling frame coincides with the usual rotating frame after one (or a few) cycle times. This restricts the possible values for the effective flip angle (Eq. [57]) of the R part of the sequence. For the design of a pulse sequence, this is an unnecessary restriction and if the performance of the pulse sequence strongly depends on fulfilling it, this, in fact, strongly limits the applicability of the methods in practice.

We now return to the RIL sequence of Fig. 3c with four refocusing pulses in the L period. We take into account also the supercycle of Fig. 1c. The separation of the refocusing pulses during the L part (see Fig. 3c) in units of the flip angle of an RF pulse of the same length is given by

$$a(s) = \left(\frac{s}{4} - 1\right)\frac{\pi}{\omega_1} \text{ and } b(s) = \left(\frac{s}{8} - 1\right)\frac{\pi}{\omega_1} \quad [63]$$

and, to place four π pulses in the L part of the RIL-ZQT cycle, s must obviously be larger than 8. In practice, this is not usually a restriction. Otherwise, the number of refocusing pulses can be reduced.

As a measure for the transfer efficiency, we use the relative size of the effective chemical-shift difference

$$\mathrm{CS}_{\mathrm{eff}} = \frac{\mathrm{tr}\{\bar{H}(S_{1z} - S_{2z})\}}{\mathrm{tr}\{(S_{1z} - S_{2z})^2\}} \quad [64]$$

with respect to the effective dipolar coupling

$$\mathrm{ZQT}_{\mathrm{eff}} = abs\,\frac{\mathrm{tr}\{\bar{H}(S_1^+ S_2^-)\}}{\mathrm{tr}\{(S_1^+ S_2^-)^2\}} \quad [65]$$

The ratio $m = \mathrm{ZQT}_{\mathrm{eff}}/\mathrm{CS}_{\mathrm{eff}}$ should be constant and maximized. Ideally, $m \to \infty$. In practice, $m \gg 1$ is sufficient. m should also be insensitive to CSA contributions and should not vary strongly with the RF amplitude. Furthermore, double-quantum contributions

$$\mathrm{DQT}_{\mathrm{eff}} = abs\,\frac{\mathrm{tr}\{\bar{H}(S_1^+ S_2^+)\}}{\mathrm{tr}\{(S_1^+ S_2^+)^2\}} \quad [66]$$

must be minimized such that the ratio $q = \mathrm{DQT}_{\mathrm{eff}}/\mathrm{ZQT}_{\mathrm{eff}}$ vanishes, or, in practice, $q \ll 1$.

As a first step, we have evaluated $\mathrm{ZQT}_{\mathrm{eff}}$, $\mathrm{DQT}_{\mathrm{eff}}$, and $\mathrm{CS}_{\mathrm{eff}}$ as a function of δ and ω_1 for a fixed MAS speed of 5 kHz and constant resonance offsets Ω_1 and Ω_2 of 5 and 0 kHz, respectively, for a single-crystal orientation with an effective dipolar coupling frequency of 130 Hz. The results are displayed in Fig. 6. The RF strength was varied between 40 and 120 kHz (assuming a CSA with an anisotropy of 3.5 and 0 kHz on spin 1 and 2, respectively, and an asymmetry of 0.5). The general trend shows an improved performance of the RIL-ZQT scheme with increasing RF field strength. The effective dipolar coupling term $\mathrm{ZQT}_{\mathrm{eff}}$ stays constant (Fig. 6a), except for some singular points where unwanted double-quantum terms appear (Fig. 6b) and the effective chemical shift $\mathrm{CS}_{\mathrm{eff}}$ contributions decrease with increasing RF field strength (Fig. 6c). The singularities appear when the effective flip angle of Eq. [57] matches a multiple of a π rotation

$$\Theta(\delta, s) = k\pi,\ k = 0, 1, 2, 3\cdots \quad [67]$$

(see Figs. 6a and 6b) in accordance with the analytical results obtained for the model pulse sequence. They lie on hyperbolic curves according to $\delta = 1 - 2k/s$ and can easily be avoided in applications. Using the simple model of the previous paragraph we can understand this phenomenon: Whenever the effective flip angle is a multiple of π, the averaging of DQT elements over several rotor cycles cannot take place and these terms remain. The size of the disturbances decreases with increasing s. It should be noted that these DQT terms do not become nonsecular with respect to an effective spin-lock field in the R part (if $\delta \neq 1$) because they originate from the L part of the pulse sequence.

Furthermore, for the RIL-ZQT sequence, enhanced effective chemical-shift-difference terms $\mathrm{CS}_{\mathrm{eff}}$ appear in the vicinity the curves $\delta = 1 - 2k/s$ for even k as seen in Fig. 6c. In addition to these sharp maxima, a smooth background that increases with decreasing δ and decreasing RF field strength is observed that comes predominantly from the first-order term of Eq. [49].

It is therefore essential to choose δ such that these unfavorable conditions are avoided. Independent of all other parameters, we can avoid all disturbances if $\Theta = (2k + 1)\pi/2$ (k is an integer), or correspondingly

$$\delta = 1 - \frac{1}{s} \text{ or } \delta = 1 - \frac{3}{s}. \quad [68]$$

The actual RF field strength where the unwanted terms are minimized can vary slightly within the limits given above. The optimum δ, e.g., for $\omega_{1,S}/2\pi = 50$ kHz, is close to the lower limit of the above range (close to $\delta = 1 - 2.5/s$) while, for $\omega_{1,S}/2\pi = 60$ kHz, the optimum δ is close to the upper limit of Eq. [68] (see Fig. 6). The limits of Eq. [68] are also included Fig. 7 where we have plotted the ratio m between effective dipolar coupling and effective chemical-shift difference. It should be noted that for $k = 1$, an unfavorable recoupling is predicted to occur. Clearly, the recoupling effects are seen in Fig. 6, but the recoupling is much smaller

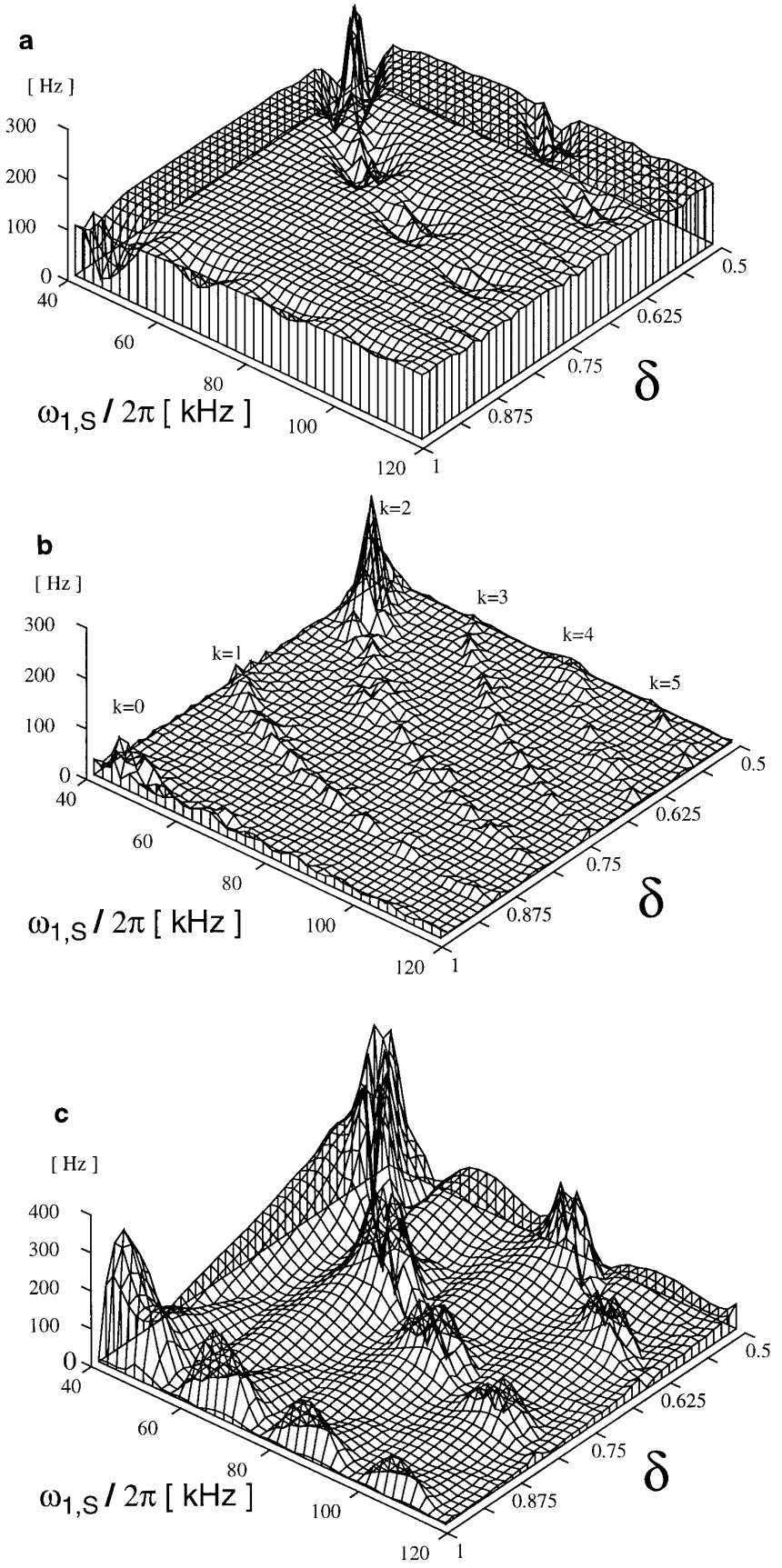

FIG. 6. Effective zero- (a) and double-quantum (b) and chemical-shift (c) contributions (as defined in Eqs. [64]–[66]) as a function of RF field strength $\omega_{1,S}$ and amplitude attenuation δ. Resonance offsets $\Omega_1 = 5$ kHz and $\Omega_2 = 0$ kHz are used. For the simulation, an arbitrary single-crystal orientation was used. Further information is given in the text.

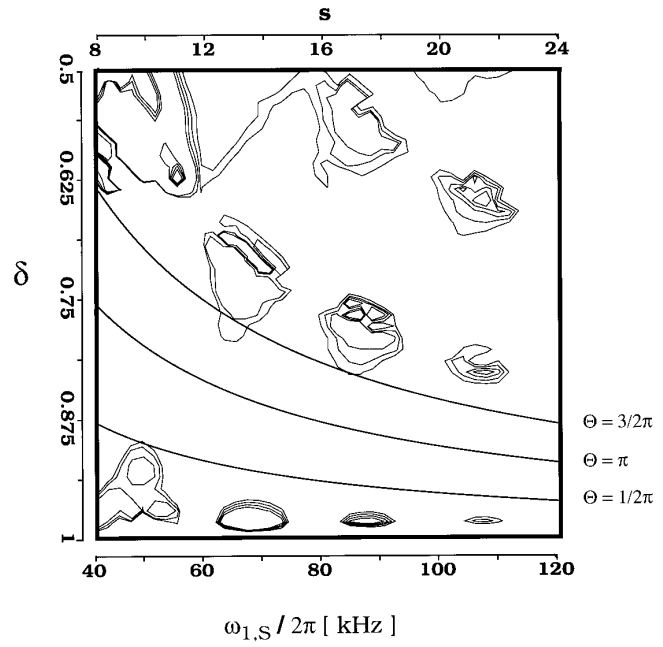

FIG. 7. Contour plot of the ratio m of effective dipolar coupling and effective chemical shift as a function of $\omega_{1,S}$ and δ. Contour levels are given for 40, 60, and 80% of the maximal value observed over the entire region. Parabolic curves correspond to effective flip angles Θ (as defined in Eq. [57]) of 0.5π, 1π, 1.5π. Ten randomly distributed single-crystal orientations were taken into account.

than that for even k values, and in practice, the odd k resonances seem to be quite unimportant. While Fig. 6 has been calculated for a specific single-crystal orientation, Fig. 7 represents a crude powder average.

So far all calculations have been performed at a fixed MAS-spinning frequency of 5 kHz. Further calculations (not shown here) show that the behavior displayed in Fig. 6 and Fig. 7 is almost independent of the MAS spinning speed if s, the ratio of RF field strength and MAS frequency, is kept constant and if the RF fields do not drop below $\omega_{1,S}/2\pi = 50$ kHz.

In Fig. 8 we finally study the isotropic chemical-shift dependence of the actual polarization transfer in a two-spin system using the optimized RIL-ZQT sequence with $\delta = 1 - 2.5/s$. Polarization was prepared on spin 1 only, $\rho(0) = S_{1z}$ and the resulting polarization on spin 2 was monitored as a function of mixing time $\langle S_{2z}\rangle = \mathrm{tr}\{\rho(\tau)S_{2z}\}$ (a) in the absence and (b) in the presence of CSA contributions. In both cases we plot the resulting signal intensity $\langle S_{2z}\rangle$ after 16 rotor cycles, which, for a coupling constant of 2 kHz and a MAS spinning speed of 5 kHz, is a measure for the initial rate of the crosspeak build-up. For (a), the CSA was neglected, and (b) a CSA with an anisotropy of 5 and 1 kHz on spin 1 and 2, respectively, was assumed. The two sets of Euler angles that describe the orientation of the CSA tensors with respect to a coordinate system whose z axis coincides with the unique principal axis of the dipolar tensor, was chosen, arbitrarily, as (10°, 20°, 30°) for spin 1 and (20°, 40°, 60°) for spin 2. For both CSA tensors, an asymmetry parameter of $\eta = 0.5$ was assumed. The isotropic chemical shifts Ω_1, Ω_2 were varied in the range of ± 20 kHz, the RF field strength was assumed to be 50 kHz. In the absence of CSA contributions (Fig. 8a) a relatively flat transfer behavior over 10–15 kHz offset is observable even for this relatively low RF field strength. In (b), where CSA interactions are included, this range diminishes to about 5–10 kHz. In both cases, performance at a higher RF field strength will increase. Increasing the number of refocusing pulses in the L part of the sequence may also improve the CSA suppression. The entire time dependence of $\langle S_{2z}\rangle$ for three particular situations out of Fig. 8, namely (i) $\Omega_1 = \Omega_2 = 0$, (ii) $\Omega_1 = 0$ and $\Omega_2 = 20$ kHz, and (iii) $\Omega_1 = \Omega_2 = -20$ kHz are displayed in Fig. 9.

4. SUMMARY OF RIL PERFORMANCE

We conclude the theoretical part by summarizing the results of the R/L optimization. For efficient application of

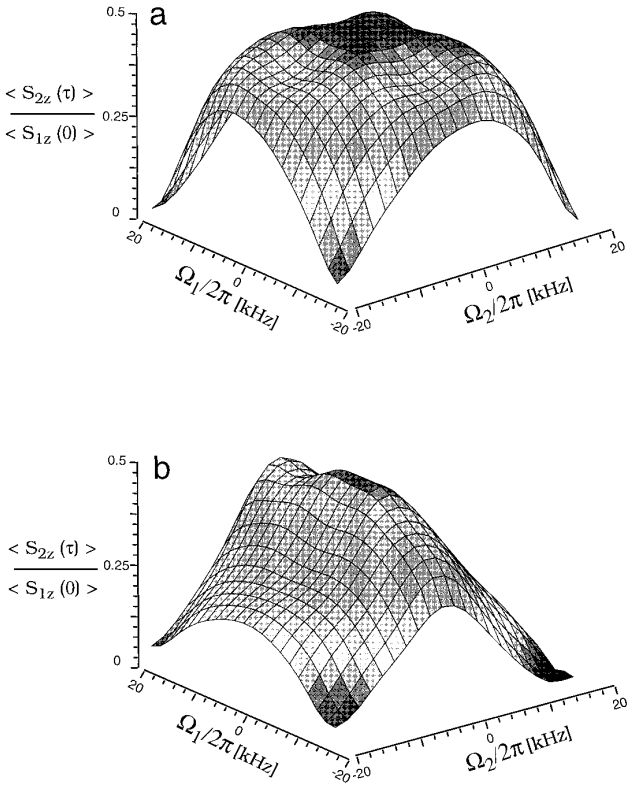

FIG. 8. Chemical-shift dependence of the transferred polarization with the optimized RIL-ZQT scheme assuming an RF field strength of 50 kHz and the correspondingly optimized amplitude attenuation δ for a powder average obtained from 100 crystal orientations for (a) vanishing CSA and (b) CSA values as given in the text. A dipolar coupling of 2 kHz was assumed. The signal $(S_{2z}(\tau))/(S_{1z}(0))$ is displayed after 8 RIL-ZQT supercycles, corresponding (using an MAS frequency of 5 kHz) to a mixing time of 3.2 ms. The isotropic chemical-shift values were varied in range of ± 20 kHz.

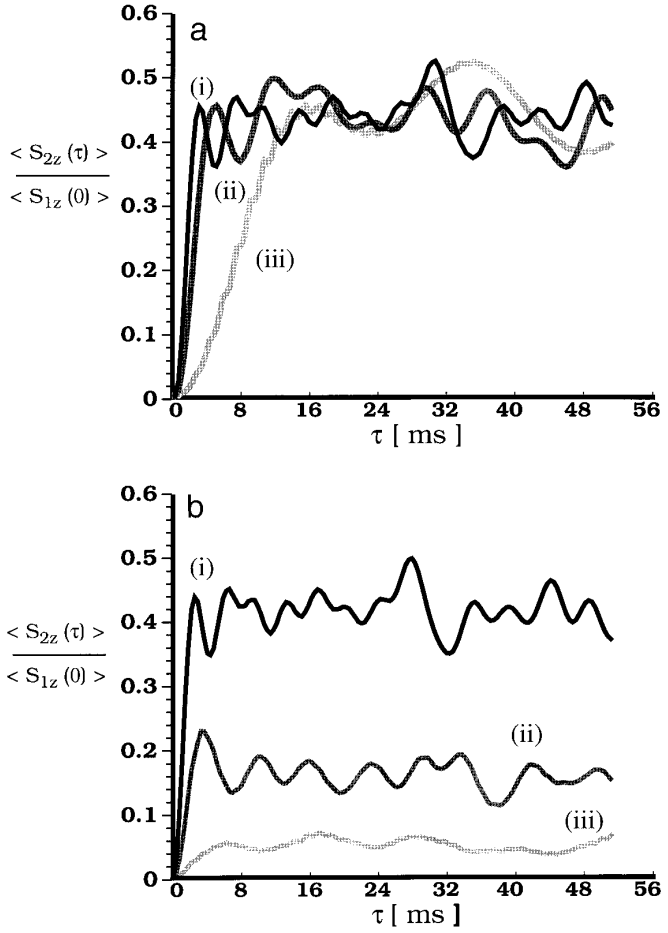

FIG. 9. Polarization transfer curves as a function of the mixing time for (i) on-resonance $\Omega_1 = \Omega_2 = 0$, (ii) $\Omega_1 = 0$ and $\Omega_2 = 20$ kHz, and (iii) $\Omega_1 = \Omega_2 = -20$ kHz using the simulation parameters described in the legend to Fig. 8. Again (a) and (b) correspond to the case of vanishing and nonvanishing CSA contributions, respectively.

the RIL-ZQT scheme the following criteria should be taken into account in the experimental setup:

(a) The R/L pulse sequence should be applied rotor-synchronously but no particular ratio of RF field strength to MAS frequency must be fulfilled.

(b) For an optimum offset compensation the RF field strength should be chosen as high as possible. For ^{13}C spectroscopy, 50–60 kHz is usually sufficient but larger values are preferred. The decoupling field strength should be as high as the ^{13}C field strength or, preferably, higher.

(c) The performance increases with $s = \omega_{1,S}/\omega_R$ which, typically, should be larger than 10 for a good compensation of CS and CSA effects.

(d) According to s, the amplitude attenuation δ should finally be set to a value close to the conditions given in Eq. [68]. This setting is not critical as long as the misadjustment does not accidentally fulfill one of the ''resonance conditions'' stated in Eq. [67] and displayed in Fig. 6b and 6c. Note that the resonances at even k are more severe. Because the resonances only depend on s, they can easily be calculated and avoided.

Unlike other proposed schemes (*24, 25, 28, 29, 31*), the RIL-ZQT makes possible the variation of the experimental parameters RF field strength and MAS spinning speed over a wide range of values. As long as one stays within the operational range indicated in Fig. 10, the ratio s can be chosen at will. The conditions used in some of the numerical calculations (e.g., that s is an integer) were only used for computational ease and are not requested in practice. The pulse sequence is therefore quite forgiving with respect to misadjustments and to RF inhomogeneities.

All cross-peak intensities are in positive adsorption irrespective of the number of spins involved in the transfer.

5. EXPERIMENTAL

The experimental section will be organized as follows. First, the improvements that can be realized by Lee–Goldburg proton decoupling will be demonstrated. Second, two-dimensional RIL-ZQT experiments in a uniformly labeled ^{13}C multispin system will be described. Third, we shall ex-

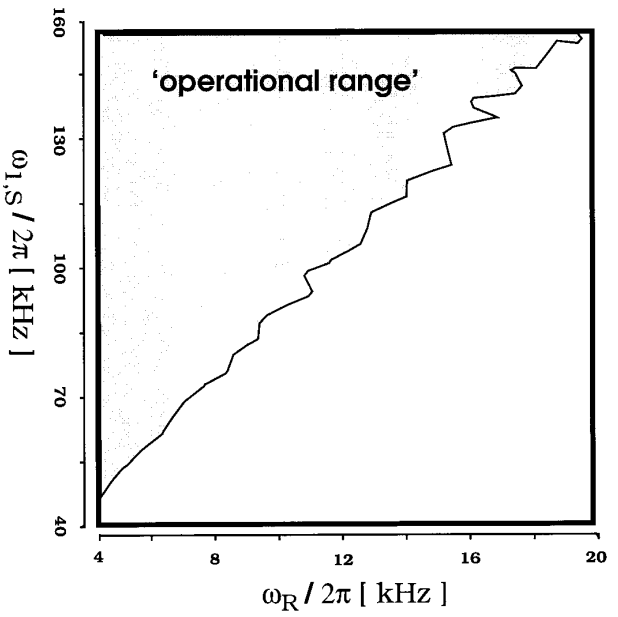

FIG. 10. Transfer efficiency as measured by the maximal transferred signal intensity on spin 2 in a two-spin system as a function of MAS spinning frequency and applied RF field strength $\omega_{1,S}$. An arbitrary single-crystal orientation was considered assuming isotropic chemical shifts of 7 and -4 kHz for spin 1 and 2, respectively. The anisotropy of the CSA tensor on spin 1 was assumed to be 2 kHz while for spin 2 CSA contributions were set to zero. The shaded area corresponds to the region where at least 85% of the maximum transfer efficiency is achieved.

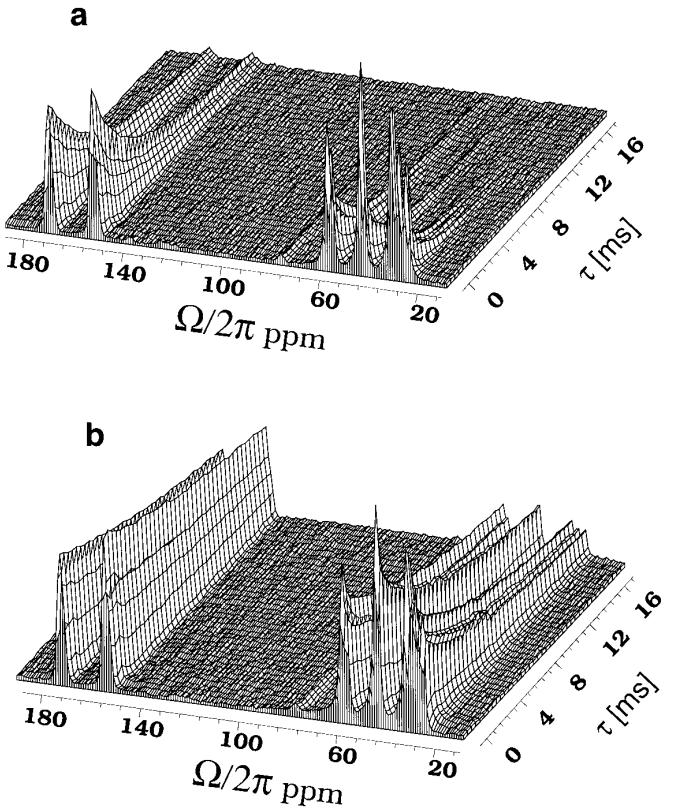

FIG. 11. Decay of the ^{13}C magnetization in a fully (^{13}C, ^{15}N)-labeled arginine powder sample during a RIL-ZQT sequence with (a) conventional on-resonance proton decoupling (DEC) and (b) with Lee–Goldburg (LG) decoupling at a RF field strength of 110 kHz. The carbon field strength of 95 kHz was used. MAS spinning was set to 9 kHz.

perimentally verify the asymmetric behavior with respect to chemical shifts predicted in the theoretical section.

5.A. Proton Decoupling

It has been pointed out in the theoretical part that the decoupling of the *I* spins from the *S* spins can be problematic. There, it was proposed to use a Lee–Goldburg decoupling scheme on the protons. In a sample with many coupled *I* spins (protons), incomplete decoupling from the protons will manifest itself as what can in a loose way be denoted as ''$T_{1\rho}$ relaxation'' of the *S* spin polarization. The decay of the ^{13}C polarization under a RIL ''spin-lock'' sequence was studied in a uniformly (^{13}C, ^{15}N)-labeled arginine powder sample. The results, obtained using a Chemagnetics Infinity spectrometer with a proton frequency of 400 MHz and a Chemagnetics standard 4-mm MAS probehead are shown in Fig. 11 for on-resonance decoupling and Lee–Goldburg decoupling at the same RF field strength of 110 kHz. The decay rate of all resonances is drastically slower in the Lee–Goldburg decoupling case (Fig. 11b) in comparison to on-resonance CW decoupling (see Fig. 11a). Similar observations were made in other contexts (*51–53*). The decay rates of the individual resonances should not be interpreted as individual $T_{1\rho}$ values as the resonances are coupled by incomplete spin-diffusion processes as shown in detail below. Furthermore, the intensity of the different resonances are not in equilibrium with each other at $\tau = 0$ due to differences in cross-polarization efficiency. The initial decay of the intensity of the individual lines under LG decoupling is expanded in Fig. 12. For the three carbon resonances with two directly bound protons, a strong initial decay of about 30% of the initial intensity is observed. We attribute this decay to incomplete decoupling of the protons which leads to the conversion of Zeeman polarization to heteronuclear dipolar order (*54*). A similar, but reduced effect is seen for the carbon resonance with one attached proton. Apparently, the pulse scheme is not completely successful to average out these strong nearest neighbor interactions. Higher decoupling fields and the application of a frequency-switched version of the Lee–Goldburg decoupling scheme (*47, 48*) might here be helpful. Nevertheless, the achieved decoupling efficiency allows us to study carbon–carbon polarization transfer at mixing times up to about 30 ms, although differential ''$T_{1\rho}$'' behavior complicates the analysis of the polarization-transfer spectra. We believe that the main source of relaxation are fluctuations of the proton spin system that lead to a relaxation of the spin-locked carbon polarization. These fluctuations become present for imperfect LG decoupling because of insufficient RF field strength and deviation from the LG condition caused by chemical shifts and RF inhomogeneity. The experiments were performed on full rotors, and a considerable RF inhomogeneity was present over the sample volume.

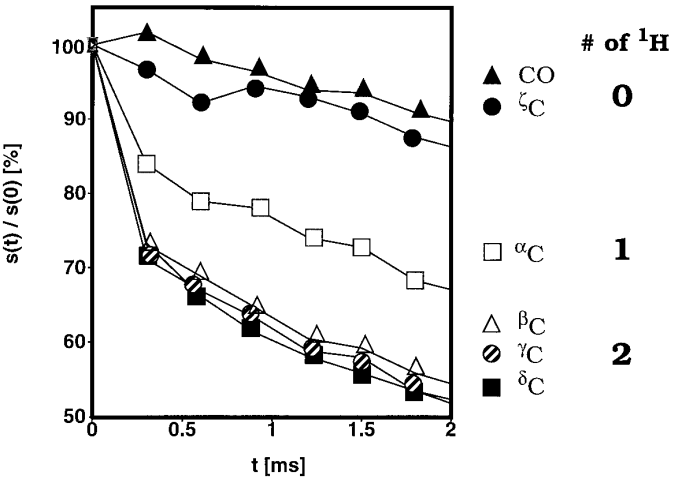

FIG. 12. Initial ^{13}C signal decay in the experiment of Fig. 11. The signal from each ^{13}C is normalized to 1 at zero mixing time. ▲, CO; ●, $^{\zeta}C$; □, $^{\alpha}C$. △, ▨, ■, $^{\beta}C$, $^{\gamma}C$, and $^{\delta}C$, respectively. Signal is normalized to 100% at zero mixing time.

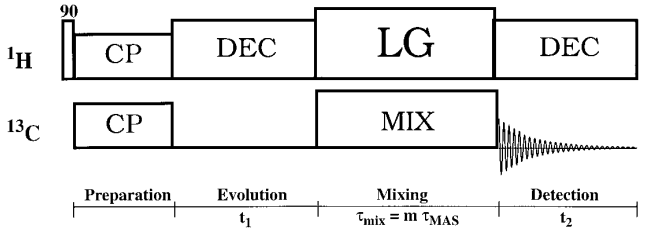

FIG. 13. Experimental scheme for a two-dimensional TOSSY experiment under MAS with Hartmann–Hahn cross polarization (CP) and on-resonance proton decoupling during evolution and detection. For mixing, the RIL-ZQT scheme as given in Fig. 3c is used under simultaneous Lee–Goldburg (see Fig. 2) decoupling.

5.B. Total Through-Space Correlation Spectroscopy

We now apply the RIL-ZQT/LG scheme to 2D total through-space correlation spectroscopy (TOSSY). The pulse scheme and experimental details are given in Fig. 13. Again, the uniformly labeled arginine test sample was used. Two-dimensional TOSSY spectra were recorded for mixing times in the range of 0–20 ms. As an example, Fig. 14

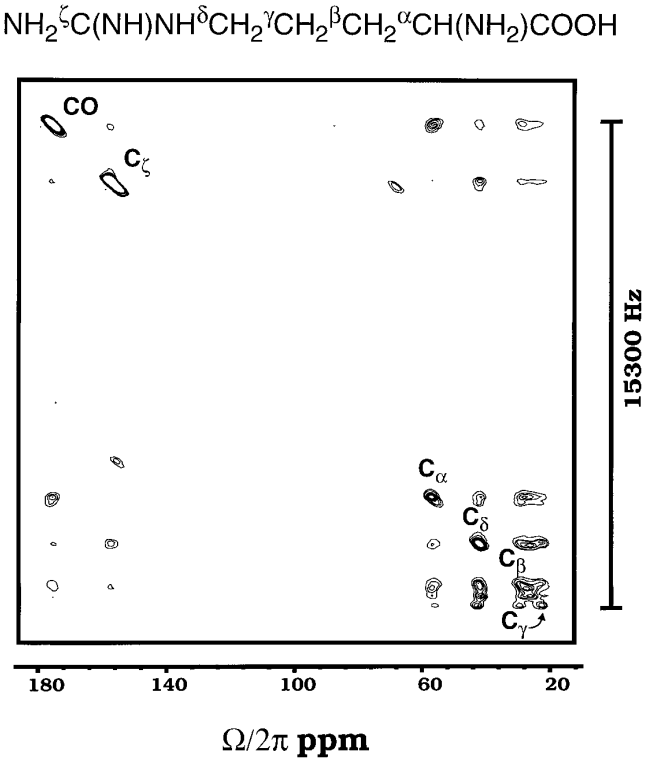

FIG. 14. Two-dimensional RIL-ZQT/LG experiment on a fully (^{13}C, ^{15}N)-labeled arginine powder sample with a mixing time of 15 ms. Due to the broadband transfer profile of the RIL-ZQT scheme, polarization transfer has occurred over the entire spectral window and all cross-peak amplitudes are in positive adsorption. An RF field strength of 95 kHz was used and a MAS spinning speed of 9.5 kHz. LG decoupling with 120 kHz field strength was employed. Contour levels are shown in linear intervals between 3 and 15% of the maximal peak intensity.

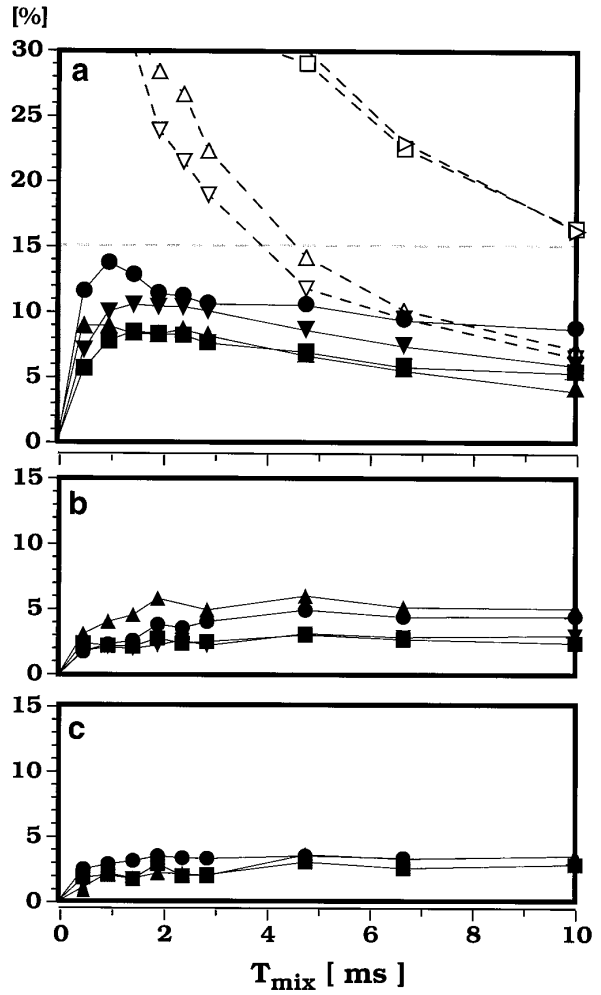

FIG. 15. Cross-peak buildup and diagonal-peak decay as a function of mixing time, normalized to the highest diagonal intensity of the 2D spectrum at zero mixing time. In the displayed time and intensity frame, diagonal- and cross-peak intensities are represented by empty and filled symbols, respectively. For the diagonal peaks, the notation □, ($^{\alpha}$C); △, ($^{\beta}$C); ▽, ($^{\gamma}$C); and ▷, ($^{\delta}$C) was used. For the one-bond cross peaks included in (a) the (CO–$^{\alpha}$C), ($^{\alpha}$C–$^{\beta}$C), ($^{\beta}$C–$^{\gamma}$C) and ($^{\gamma}$C–$^{\delta}$C) are represented by ●, ■, ▲, ▼, respectively. In the same symbolic order, selected two-bond couplings in (b) represent the pairs CO–$^{\beta}$C, $^{\alpha}$C–$^{\gamma}$C, $^{\beta}$C–$^{\delta}$C, and $^{\gamma}$C–$^{\zeta}$C. Finally, cross-peak intensities for some of the observable three-bond connectivities such as CO–$^{\gamma}$C (●), $^{\alpha}$C–$^{\delta}$C (■), and $^{\beta}$C–$^{\zeta}$C (▲) are shown. All experimental spectra were recorded using a carbon field strength of 75 kHz and a LG proton decoupling strength of 100 kHz. An MAS spinning speed of 7 kHz was used.

displays the phase-sensitive TOSSY spectrum obtained at a mixing time of 15 ms. The crosspeak amplitudes as a function of the mixing time are plotted in Fig. 15. Figure 15a contains the buildup curves for directly bound carbon resonances with a dipole coupling constant exceeding 2 kHz. The cross-peak buildup is counteracted by the $T_{1\rho}$ relaxation. Also given in Fig. 15a is the decay of the diagonal peaks of the methylene carbons. For longer mixing time (>5 ms), cross-peak intensities between methylene resonances ap-

proach the intensity of the diagonal peaks, indicating complete polarization transfer. The relative amplitudes of the cross peaks between the different carbon resonances are difficult to compare due to the differential $T_{1\rho}$ relaxation of the diagonal peaks. The rate constants of the signal buildup are, however, all comparable as expected because all pairs have similar dipole coupling constants. The large difference in chemical-shift differences between the resonances involved (from 1 to 15.3 kHz) does not considerably influence the rate constants. The maximum cross-peak amplitude has been reached after about 2 to 2.5 ms for all one-bond carbon pairs considered in Fig. 15a. Exact numerical simulations for an isolated single-bond carbon–carbon two-spin system (see, e.g., Fig. 9) lead to a value of 3 ms. However, care must be applied to quantitatively interpret these positions due to the interference with relaxation (especially in the CO–C_α pair) and neighboring coupling partners. The effect of relaxation upon the effective cross-peak amplitudes as a function of mixing time may be further elucidated by performing RIL–LIR control experiments (*42, 43*) in which the dipolar mixing process is refocused.

While the ratio of cross- to diagonal-peak intensity approaches one for the methylene groups the absolute cross-peak intensity with respect to the initial diagonal-peak intensity (at zero mixing time) does not exceed 15% due to relaxation. Higher absolute efficiencies have been found by us and others for two-spin systems with smaller dipolar interactions, e.g., in zinc acetate (*26, 28*) where relaxation is less severe. A complete spin diffusion between all resonances would lead to 36 peaks of equal height, 17% on our scale. The cross-peak intensity between resonances of carbon spins separated by two atomic bonds is given in Fig. 15b, cross peaks between further peaks are given in Fig. 15c. Here the cross-peak buildup is slower and no clear maximum can be evaluated. As in all total correlation spectra, the interpretation of small cross peaks in the presence of larger cross peaks is difficult because direct as well as relayed transfer mechanisms are involved. Furthermore, spins pairs with strong mutual couplings may not exchange polarization with weakly coupled neighbors due to ''spectral detuning'' effects (*17*).

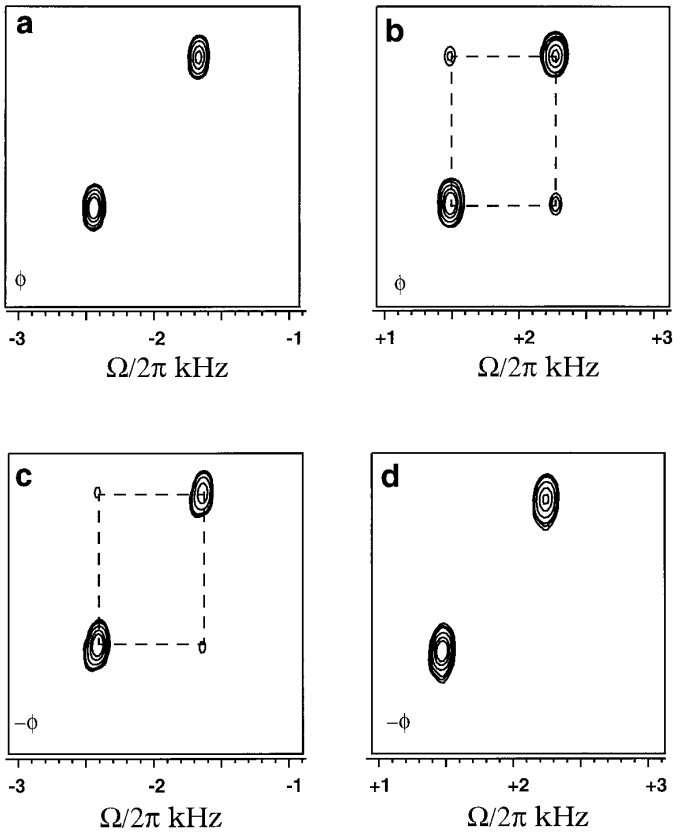

FIG. 16. Polarization-transfer experiment on a powdered sample of adamantane (natural abundance ^{13}C) using the pulse sequence of Fig. 4a without a supercycle. The chemical shift, measured with respect to the carrier frequency is positive for both resonances in (b) and (d) and negative in (a) and (c). The spectra (c, d) were taken with an inverted RF phase for the *y* pulses. As predicted in the theoretical section, the spectra are asymmetric with respect to a sign change of the chemical shift (with respect to the carrier). A phase change of the *y* pulses inverses the asymmetry. The contour levels were set to 5, 10, . . . , 75% of the maximal diagonal intensity.

5.C. Frequency Selective R/L-Transfer

In Section 3, we have seen that under finite RF strength conditions higher order recoupling terms appear that depend on the sign of (a) the resonance offsets and (b) the phase of the *y* pulses of the L part. Here, we demonstrate experimentally the presence of the asymmetry predicted in the theoretical part. To this end, we have performed a test experiment on a sample of adamantane with ^{13}C at natural abundance with the pulse sequence of Fig. 3a with $\omega_1/2\pi = 50$ kHz at $\omega_R = 5$ kHz. We have varied the isotropic resonance offset of both resonances by placing the carrier frequency at −2 kHz (Fig. 16a) or +2 kHz (Fig. 16b) with respect to the center between the two resonances, thereby changing the sign of the resonance offset of both resonances, Ω_1 and Ω_2. Both experiments were also performed with the sign of the phase ϕ of all pulses in the L part inverted (see Figs. 16c and 16d). For a constant mixing time of 45 ms we observe substantial cross peaks in Figs. 16b and 16c while they are missing in Figs. 16a and 16d, thus confirming the theoretical predictions. This might be exploited in the context of ''tailored'' TOSSY experiments, in analogy to the tailored polarization transfer schemes (*55, 56*) used in liquid-state total correlation spectroscopy.

6. CONCLUSIONS

In this article we have used average Hamiltonian theory and numerical simulations to study and optimize homonu-

clear broadband polarization transfer under MAS with efficient proton decoupling. The pulse sequences presented here extend the upper limit of the observation window for ^{13}C polarization transfer in organic solids with strongly coupled protons under MAS to typically 20 ms. The RIL pulse sequence used is not based on a matching between RF field amplitude and spinning frequency but can be applied over a wide range of values for these two parameters. This renders the experiment also less sensitive to RF inhomogeneity and amplitude fluctuations. However, the pulse-sequence timing (the cycle time) must be synchronized approximately with the MAS frequency. This condition is, however, easily fulfilled in practical applications.

In the theoretical part, analytical expressions for the R/L driven transfer schemes under finite RF conditions are given. The influence of higher order AHT terms, often neglected in the design of recoupling pulse sequences, was found to strongly influence the pulse-scheme performance. These effects can also lead to an asymmetry (with respect to an inversion of the sign of the chemical shifts) of the cross-peak intensity in polarization-transfer spectra. This behavior was experimentally verified and can possibly be useful in designing tailored pulse schemes that enhance polarization transfer under spinning conditions only among spin subsystems of interest.

The initial rate of the cross-peak buildup was compared to the internuclear distances known from X-ray crystallography. Qualitative agreement was observed and high rate constants correlate with the shortest distances. Cross-peak buildup also occurs for longer distances where it can be used to establish neighborhoods over distances of up to 10 Å. For these ''long-range'' interactions, the elucidation of distances is complicated due to the presence of direct and relayed transfer. Nevertheless, the R/L approach can be used to obtain valuable structural information in multispin systems as recently demonstrated by Sebald and co-workers (*57*) in a ^{31}P model system.

The optimized RIL-ZQT/LG scheme presented allows total through-space correlation under MAS conditions for a variety of experimental settings. We judge the performance of the optimized RIL/ZQT pulse-sequence with respect to the parameters of the ^{13}C spin system as sufficiently good for applications. The polarization decay caused by the bath of surrounding proton spins is still fast enough to prevent a precise determination of internuclear distances. Improvements are highly desirable and work along these lines is in progress.

APPENDIX A

For the pulse scheme of Fig. 3a anisotropic dipolar and chemical shielding interaction are modulated by the MAS spinning and depend, in the R part, on the ratio of RF field strength and MAS frequency s. For the zeroth-order AH contribution of the R part we find, assuming s to be an even integer,

$$\bar{H}^{(0)}_{S,\mathrm{CSA}} = \sum_k \frac{2\gamma_k B_0}{3\pi\sqrt{2}}\,\delta_k \sin(\theta_k)(a_{kx}S_{kx} + a_{ky}S_{ky}) \quad [A1]$$

and

$$\bar{H}^{(0)}_{IS,D} = \sum_{k<l} \frac{2d^{(k,l)}}{\sqrt{2}\pi}\sin(2\theta^{(kl)})\left[\frac{s}{s^2-1}\cos(\varphi^{(kl)})S_{ky} - \frac{1}{s^2-1}\sin(\varphi^{(kl)})S_{kx}\right]\frac{1}{\sqrt{3}}I_{lz}, \quad [A2]$$

where

$$\begin{aligned} a_{kx} &= \frac{1}{s^2-1}[\sin(\varphi_k)(3-\eta_k\cos(2\chi_k))\cos(\theta_k) \\ &\quad + \cos(\varphi_k)\eta_k\sin(2\chi_k)] \\ a_{ky} &= \frac{s}{s^2-1}[\cos(\varphi_k)(3-\eta_k\cos(2\chi_k))\cos(\theta_k) \\ &\quad - \sin(\varphi_k)\eta_k\sin(2\chi_k)] \end{aligned} \quad [A3]$$

All terms are inversely proportional to s or s^2 and can be neglected for strong RF fields.

APPENDIX B

The coefficients of Eq. [54] read as

$$\begin{aligned} a^{(0)}(\theta,\varphi) &\approx b(0.348\,\sin(2\theta)\sin(\varphi) \\ &\quad - 0.078\,\sin^2\theta\cos(2\varphi)) \\ a^{(2)}(\theta,\varphi) &\approx b(0.131\,\sin(2\theta)\sin(\varphi) \\ &\quad + 0.078\,\sin^2\theta\cos(2\varphi)) \\ a^{(z)}(\theta,\varphi) &\approx (-b)(0.348\,\sin(2\theta)\sin(\varphi) \\ &\quad + 0.078\,\sin^2\theta\cos(2\varphi)) \\ a^{(1,x)}(\theta,\varphi) &\approx b(0.021\,\sin(2\theta)\sin(\varphi) \\ &\quad + 0.001\,\sin^2\theta\cos(2\varphi)) \\ a^{(1,y)}(\theta,\varphi) &\approx 0.024b\,\sin(2\theta)\cos(\varphi) \end{aligned} \quad [B1]$$

and depend on the effective dipolar coupling b and the Euler angles θ and φ used in Eq. [7].

APPENDIX C

The coefficients $A_{\alpha,\beta}$ of Eq. [56] are given by

$$\begin{aligned} A_{\alpha,\beta} &= a_{\alpha,\beta}\Omega_1 + b_{\alpha,\beta}\Omega_2 \\ A_{\beta,\alpha} &= b_{\alpha,\beta}\Omega_1 + a_{\alpha,\beta}\Omega_2 \end{aligned} \quad [C1]$$

with

$$
\begin{aligned}
a_{x,y} \approx\ & (1.672\cos\varphi + 0.102\sin\varphi)\sin(2\theta) \\
& + (1/\sqrt{2})(2.022\cos 2\varphi \\
& \quad + 1.554\sin 2\varphi)\sin^2\theta \\
b_{x,y} \approx\ & ((-1.521)\cos\varphi + 1.185\sin\varphi)\sin(2\theta) \\
& + (1/\sqrt{2})((-2.168)\cos 2\varphi \\
& \quad + 0.434\sin 2\varphi)\sin^2\theta \\
a_{x,z} \approx\ & (-0.321)\sin\varphi\sin(2\theta) \\
b_{x,z} \approx\ & (0.007\cos\varphi + 0.175\sin\varphi)\sin 2\theta \\
a_{y,z} \approx\ & (-1)(0.144\cos\varphi + 0.301\sin\varphi)\sin(2\theta) \\
& + (1/\sqrt{2})(0.188\cos 2\varphi \\
& \quad + 0.165\sin 2\varphi)\sin^2\theta \\
b_{y,z} \approx\ & ((-0.005)\cos\varphi - 0.202\sin\varphi)\sin(2\theta) \\
& + (1/\sqrt{2})(0.064\cos 2\varphi \\
& \quad - 0.004\sin 2\varphi)\sin^2\theta. \qquad [C2]
\end{aligned}
$$

The angular dependence described by the Euler angles θ, φ results from the dipolar coupling. Finally, we give the coefficients of the first-order dipole–dipole cross term in Eq. [56]:

$$
\begin{aligned}
B_x \approx\ & \frac{[\sin(2\theta)^2(13\cos(2\varphi) - 8\sin(2\varphi) + 12) \\
& \quad + \sin(2\theta)\sin^2(\theta)(6\sin(\varphi) - 4\cos(\varphi) \\
& \qquad + 4\sin(3\varphi) + 2\cos(3\varphi))]}{1000} \\
B_y \approx\ & \frac{[\sin(2\theta)^2(0.8\cos(2\varphi) - 70\sin(2\varphi) + 880) \\
& \quad - \sin(2\theta)\sin^2(\theta)(660\cos(\varphi) + 220\sin(\varphi) \\
& \qquad - 100\sin(3\varphi) - 210\cos(3\varphi))]}{1000} \\
B_z \approx\ & \frac{[\sin(2\theta)^2(160\cos(2\varphi) - 90\sin(2\varphi) + 710) \\
& \quad - \sin(2\theta)\sin^2(\theta)(82\cos(\varphi) + 212\sin(\varphi) \\
& \qquad - 42\sin(3\varphi) + 48\cos(3\varphi))]}{1000}.
\end{aligned}
\qquad [C3]
$$

ACKNOWLEDGMENTS

Support from SON and the SON National HF-NMR Facility, University of Nijmegen and excellent technical support by J. van Os, H. Jannsen, and G. Nachtegaal are gratefully acknowledged. We thank Prof. Dr. R. R. Ernst for his interest and support. Scientific discussions with D. G. Geurts, Dr. A. P. M. Kentgens, Dr. R. J. Iuliucci, and Dr. M. Tomaselli have been helpful.

REFERENCES

1. R. R. Ernst, G. Bodenhausen, and A. Wokaun, ''Principles of Nuclear Magnetic Resonance in One and Two Dimensions,'' Clarendon Press, Oxford (1987).
2. K. Wüthrich, ''NMR of Proteins and Nucleic Acids,'' Wiley–Interscience, New York (1986).
3. K. Schmidt-Rohr and H. W. Spiess, ''Multidimensional Solid-State NMR and Polymers,'' Academic Press, London (1994).
4. J. Jeener, B. H. Meier, P. Bachmann, and R. R. Ernst, *J. Chem. Phys.* **71,** 4546 (1979).
5. W. P. Aue, E. Bartholdi, and R. R. Ernst, *J. Chem. Phys.* **64,** 2229 (1976).
6. L. Braunschweiler and R. R. Ernst, *J. Magn. Reson.* **53,** 521 (1983).
7. E. R. Andrew, A. Bradbury, and R. G. Eades, *Nature (London)* **182,** 1659 (1958).
8. M. G. Colombo, B. H. Meier, and R. R. Ernst, *Chem. Phys. Lett.* **146,** 189 (1988).
9. M. H. Levitt, *J. Chem. Phys.* **88,** 3481 (1988).
10. D. P. Raleigh, A. C. Kolbert, T. G. Oas, M. H. Levitt, and R. G. Griffin, *J. Chem. Soc. Faraday Trans.* **84,** 3691 (1988).
11. M. H. Levitt, D. P. Raleigh, F. Creuzet, and R. G. Griffin, *J. Chem. Phys.* **92,** 6347 (1990).
12. R. G. S. Spencer, K. W. Fishbein, M. H. Levitt, and R. G. Griffin, *J. Chem. Phys.* **100,** 5533 (1994).
13. F. Creuzet, A. McDermott, R. Gebhard, K. van der Hoef, M. B. Spijker-Assink, J. Herzfeld, J. Lugtenburg, M. H. Levitt, and R. G. Griffin, *Science* **251,** 783 (1991).
14. A. E. McDermott, F. Creuzet, R. Gebhard, K. van der Hoef, M. H. Levitt, J. Herzfeld, J. Lugtenburg, and R. G. Griffin, *Biochemistry* **33,** 6129 (1994).
15. O. B. Peersen, M. Groesbeek, S. Aimoto, and S. O. Smith, *J. Am. Chem. Soc.* **117,** 7228 (1995).
16. P. T. Lansbury, P. R. Costa, J. M. Griffiths, E. J. Simon, M. Auger, K. J. Halverson, D. A. Kocisko, Z. S. Hendsch, T. T. Ashburn, R. G. S. Spencer, B. Tidor, and R. G. Griffin, *Nature Struct. Biol.* **2,** 990 (1995).
17. B. H. Meier, *Adv. Magn. Opt. Reson.* **18,** 1 (1994).
18. M. Tomaselli, B. H. Meier, M. Baldus, J. Eisenegger, and R. R. Ernst, *Chem. Phys. Lett.* **225,** 131 (1994).
19. R. Tycko, *J. Am. Chem. Soc.* **116,** 2217 (1994).
20. R. Tycko and G. Dabbagh, *Chem. Phys. Lett.* **173,** 461 (1990).
21. T. Gullion and S. Vega, *Chem. Phys. Lett.* **194,** 423 (1992).
22. R. Tycko and S. O. Smith, *J. Chem. Phys.* **98,** 932 (1993).
23. A. E. Bennett, J. H. Ok, R. G. Griffin, and S. Vega, *J. Chem. Phys.* **96,** 8624 (1992).
24. T. Fujiwara, A. Ramamoorthy, K. Nagayama, K. Hioka, and T. Fujito, *Chem. Phys. Lett.* **212,** 81 (1993).
25. N. C. Nielsen, H. Bildsoe, H. J. Jakobsen, and M. H. Levitt, *J. Chem. Phys.* **101,** 1805 (1994).
26. M. Baldus, M. Tomaselli, B. H. Meier, and R. R. Ernst, *Chem. Phys. Lett.* **230,** 329 (1994).
27. J. M. Joers, R. Rosanske, T. Gullion, and J. R. Garbow, *J. Magn. Reson. A* **106,** 123 (1994).
28. Y. K. Lee, N. D. Kurur, M. Helmle, O. G. Johannessen, N. C. Nielsen, and M. H. Levitt, *Chem. Phys. Lett.* **242,** 304 (1995).
29. B. Q. Sun, P. R. Costa, D. Kocisko, P. T. Lansbury, and R. G. Griffin, *J. Chem. Phys.* **102,** 702 (1995).

30. D. M. Gregory, D. J. Mitchell, J. A. Stringer, S. Kiihne, J. C. Shiels, J. Callahan, M. A. Metha, and G. P. Drobny, *Chem. Phys. Lett.* **246,** 654 (1995).

31. T. Fujiwara, K. Sugase, M. Kainosho, A. Ono, A. Ono, and H. Akutsu, *J. Am. Chem. Soc.* **117,** 11,351 (1995).

32. U. Haeberlen, High resolution NMR in solids: Selective averaging, *in* ''Advances in Magnetic Resonance,'' Supplement 1, Academic Press, New York, 1976.

33. M. M. Maricq, *Adv. Magn. Reson.* **14,** 151 (1990).

34. M. Mehring, ''Principles of High Resolution NMR in Solids,'' 2nd ed., Springer-Verlag, Berlin (1983).

35. W. Magnus, *Commun. Pure Appl. Math.* **7,** 649 (1954).

36. W. K. Rhim, A. Pines, and J. S. Waugh, *Phys. Rev. Lett.* **25,** 218 (1970).

37. W. K. Rhim, A. Pines, and J. S. Waugh, *Phys. Rev. B* **3,** 684 (1971).

38. H. Schneider and H. Schmiedel, *Phys. Lett. A* **30,** 298 (1969).

39. S. Zhang, B. H. Meier, and R. R. Ernst, *Phys. Rev. Lett.* **69,** 2149 (1992).

40. B. H. Meier and W. L. Earl, *J. Chem. Phys.* **85,** 4905 (1986).

41. B. H. Meier and W. L. Earl, *J. Am. Chem. Soc.* **109,** (1987).

42. R. R. Ernst, 37th ENC conference, Pacific Grove, California, 1996.

43. M. Tomaselli, ''Development and Application of Some NMR Experiments for Studying Disordered Solids,'' Ph.D. thesis No. 11455, ETH Zürich, 1996.

44. M. M. Maricq and J. S. Waugh, *J. Chem. Phys.* **70,** 3300 (1979).

45. M. Lee and W. I. Goldburg, *Phys. Rev. A* **140,** 1261 (1965).

46. M. Goldman, P. J. Grandinetti, A. Llor, Z. Olejniczak, J. R. Sachleben, and J. W. Zwanziger, *J. Chem. Phys.* **97,** 8947 (1992).

47. A. Bielecki, A. C. Kolbert, and M. H. Levitt, *Chem. Phys. Lett.* **155,** 341 (1989).

48. A. Bielecki, A. C. Kolbert, H. J. M. de Groot, R. G. Griffin, and M. H. Levitt, *Adv. Magn. Reson.* **14,** 111 (1990).

49. S. Hediger, B. H. Meier, and R. R. Ernst, *J. Chem. Phys.* **102,** 4000 (1995).

50. S. A. Smith, T. O. Levante, B. H. Meier, and R. R. Ernst, *J. Magn. Reson. A* **106,** 75 (1994).

51. M. Baldus, D. G. Geurts, S. Hediger, and B. H. Meier, *J. Magn. Reson. A* **118,** 140 (1996).

52. M. Baldus and B. H. Meier, *J. Magn. Reson. A* **121,** 65 (1996).

53. M. Baldus, R. J. Iuliucci, and B. H. Meier, *J. Am. Chem. Soc.* **119,** 1121 (1997).

54. S. Zhang, B. H. Meier, and R. R. Ernst, *Solid State Nucl. Magn. Reson.* **1,** 313 (1992).

55. S. J. Glaser and G. P. Drobny, *Chem. Phys. Lett.* **164,** 456 (1989).

56. S. J. Glaser and G. P. Drobny, *Adv. Magn. Reson.* **14,** 35 (1990).

57. S. Dusold, J. Kümmerlen, T. Schaller, A. Sebald, and W. A. Dollase, *J. Phys. Chem.* (1997), in press.